https://doi.org/10.1016/j.jcsr.2020.106438

Effect of access openings on the buckling performance of square hollow section module stub columns

Tekcham Gishan Singh, Tak-Ming Chan*

Department of Civil and Environmental Engineering, The Hong Kong Polytechnic University, Hung Hom, Hong Kong, China

Abstract

This paper presents a systematic finite element (FE) based parametric study to quantify the buckling capacity of perforated cold-formed and hot-rolled steel module column. The effects of various key geometric parameters such as eccentricity (location of perforation/column length), shapes (*viz.* circular, square and hexagonal), sizes (width/diameter) and height (depth) of perforation; and cross-sectional thickness, on the buckling performance of cold-formed and hot-rolled steel stub columns, have been investigated. Based on the analysis, the reduction in column capacity is found to be maximum when the perforation is located at column mid-height, as anticipated. The perforation shapes under consideration have been found to have marginal impact on the buckling capacity of the module stub columns, although the reduction in column capacity is seen to be in the order – square > hexagon > circular perforated columns (having same perforation size). The critical buckling capacity of perforated module column is observed to be linearly decreasing as the perforation size ratio (perforation size/flat-element width) increases. However, for the same width of perforation, increasing the perforation height up to 2.5 times the perforation width, the change in column capacity is found to be negligible. Furthermore, the applicability of existing design equations for perforated columns has been assessed and found that, although most of the design equations generate conservative and reliable predictions both for cold-formed and hot-rolled steel, the design formulae which are based on effective width method are found to be more accurate as compared to those which are based on total area method.

Keywords: Module column; Perforation/cut-outs/holes; Local buckling; Perforation eccentricity; Perforation size, Perforation shape; Perforation height; Cold-formed and hot-rolled steel; Finite element analysis; Design equations.

* Corresponding author at: Department of Civil and Environmental Engineering, The Hong Kong Polytechnic University, Hung Hom, Hong Kong, China.
E-mail address: tak-ming.chan@polyu.edu.hk (T.-M. Chan).

1 Introduction

Owing to their superiority in quality and speedy construction, the off-site prefabricated factory manufactured volumetric constructions, popularly known as modular steel construction (MSC), has attracted extensive interest both for engineers and researchers in the recent years. In MSC, inter-module connections play an important role in successful structural stability of the assembled modules. Steel bolted connections are preferred choice as it allows modules to be connected from the inside of the module and avoid additional site installation requirements, as compared to site-welding and composite concrete-steel connections [1–3]. Perforations (cut-outs/holes/openings) of different shapes (e.g. circular, rectangular, hexagonal, flat-ovals etc.,) and sizes are made on the module columns to provide access for inter-module connection, as shown in Fig. 1 (a) [4,5]. Additionally, perforations are also made on the structural member, may be for permanent or temporary access, for various needs such as duct work; bridging; connection to other members; aesthetic appearance; material optimisation as well as various services *viz*., inspections, hidden electrical and signal wiring, fresh and waste-water plumbing etc., as shown in Fig.1 (b) [6]. However, due to the introduction of perforation, structural stability and performance of columns are expected to be affected. Hence, it is imperative to study the influence of various form of perforation(s) on the overall performance of a structural member for effective use of constructional steel material and design, while satisfying the needs (e.g. duct work; bridging; connection to other members; aesthetic appearance; material optimisation as well as various services *viz*., inspections, hidden electrical and signal wiring, fresh and waste-water plumbing etc.).

In the literature, extensive studies been reported indicating the reduction in capacity and overall stability of plates [7–13], beams [14–20], columns [21–30], and members under pure torsion [31,32], due to the presence of various forms of perforations/cut-outs. An experimental study to investigate symmetric progressive buckling load of thin–walled mild steel square tubes with circular perforations, has been conducted by Marshall and Nurick [21] and further reported a linear decrease in the buckling load as the perforation diameter increases. Jullien and Limam [22] performed an experimental and numerical programme to study the stability of cylindrical shells having square, rectangular, circular cut-outs, under axial compression, and reported that the buckling load of identical shells having different perforation shapes with equal cut-out width are same. Shanmugam et al. [9] studied post-buckling behaviour and the ultimate load capacity of perforated plates, considering various parameters including plate slenderness, opening size, boundary conditions and the nature of loading, and reported that plates with circular perforations have higher capacities as compared to those with square perforations. Later, a design formula to determine the ultimate load carrying capacity of perforated plate was established using the column capacities generated from the finite element (FE) analyses. Dhanalakshmi and Shanmugam [25] reported a test programme on the axial capacity of perforated cold-formed steel angles subjected to axial compressive loading and concluded that, an approximately 50% reduction in ultimate capacity for 60% perforation, while the reduction was found to be negligible for 20% perforation. Further, using the column capacities generated from the test and parametric study, a simplified design formula as a function of plate slenderness ratio, opening size ratio, and ultimate to squash load ratio was proposed, to determine the ultimate capacity of angle stub columns having single or multiple openings. Shanmugam and Dhanalakshmi [24] established a design formula to predict the ultimate load capacity of short channel columns containing single or multiple openings of square, circular and manufacturer's perforation, utilizing the column capacities generated from an extensive parametric study using FE analysis. Moen and Schafer [33] experimentally and numerically studied the influence of slotted perforations on the local, distortional, and global elastic buckling response of short and intermediate C-section columns. It was shown that the presence of slotted perforations slightly decreases the ultimate column capacity, however, the perforation could change the post-peak ductility and buckling deformation of the member. Using iso-parametric spline finite strip method (ISFSM), Yao and Rasmussen [26] studied inelastic behaviour of perforated thin single plates and C-sections subjected to uniform compression for a range of geometric parameters namely hole shapes, sizes, length and spacings. Based on the analysis it was reported that the influence of perforation shapes, length and spacing are lesser as compared to perforation width as it offers major contribution in the effective area of the cross-section. Kunal et al. [27] studied the effect of single circular perforation on the ultimate buckling load of a circular lean duplex stainless steel (LDSS) stub column loaded axially using numerical tools and further observed that the decrease in critical buckling load of perforated column is maximum when the perforation is located at column mid-height. Singh and Singh [29] performed an experimental programme to quantify the capacity of stub column having two opposite central circular perforation located at mid-height of column and key results of the study will be discussed briefly in Section 2 of this paper. Feng et al. [30] conducted an experimental study on pin-ended aluminium alloy squares (SHSs) and rectangular hollow sections (RHSs) containing single and multiple circular openings at two opposite sides of the cross-section. Based on the test results it was concluded the reduction in elastic stiffness, ultimate load and ductility of the perforated aluminium alloy columns generally increases with decreasing perforation size and number of circular openings. Further, the experimental investigation was complimented with a series of numerical investigations in Feng et al. [34], focusing on wider range of different cross-section dimensions, overall lengths, as well as diameters, numbers, and locations of circular perforations. It was reported that, the influence of location of the perforation on the ultimate strengths of perforated aluminium alloy columns are less significant.

From the above brief literature review it has been witnessed that, although the effect of several key geometric parameters, *viz.*, perforation shape, size (width or diameter), depth (height or length), eccentricity (location), number etc., on the structural performance of perforated column has been reported, most of published literatures are mainly based on plates, opened section, and circular hollow sections (cylindrical shells); and sections made from aluminium alloys. However, to the best of authors' knowledge, there is an apparent lack of systematic investigation on the critical buckling capacity of stub module column having a single perforation on one side of the SHS, considering both cold-formed and hot-rolled steels. Hence, in this paper, a comprehensive study on the effect of perforation eccentricity, shapes (circular, square and hexagonal), width and depth; and cross-sectional thickness on the critical buckling performance of perforated module column has been attempted through validated non-linear FE approach. Initially, a brief summary of experimental programme on perforated cold-formed steel SHS and RHS, reported by Singh and Singh [29] has been presented in Section 2. Further, in Section 3, FE models have been developed and verify the modelling procedure of perforated stub column using the test results [29]. Upon validation of the FE modelling procedures, material models of cold-formed [35] and hot-rolled [36] steels for probable parametric study has been briefly discussed. The stress-strain curves generated from the material models [35,36] have been validated against the existing measured test results for S355 cold-formed and hot-rolled steel respectively reported by Nseir [37] and Liew [38]. Further, using the validated numerical modelling procedure and material models, parametric study has been conducted considering key geometric parameters influencing perforated column capacity and discussion of the FE results generated from the parametric study has been reported. Finally, the applicability of the existing design equations for perforated steel compression member detailed in AISI S100-16 [39] and those proposed by researchers [9,24,25,40,41] has been assessed for design of cold-formed and hot-rolled steel stub module columns having single perforation. Reliability analysis has been conducted to evaluate the accurateness of the design equations.

2 Summary of experimental investigation

In this section, a brief summary of the experimental investigation on the ultimate capacity of perforated cold-formed steel tubular stub columns conducted by Singh and Singh [29] is presented. A total of 31 concentrically loaded stub column tests were performed, considering five different RHSs, and two opposite central circular perforations of various sizes (perforation diameter to flat element width ratios ranging from 0.1 to 0.9). The study predominantly focused on the effect of perforation size on the local buckling capacity of columns, considering YSt-310 cold-formed steel hollow sections, manufactured by Tata Steel India commercially available in the market with the brand name – *Tata Structura YSt-310* [42]. The steel material has nominal yield stress and tensile strength of 310 MPa and 450 MPa respectively, and minimum elongation at fracture of 10%, conforming to Indian Standard 4923 [43]. The study also developed an imperfection amplitude formula for perforated cold-formed steel, based on the original imperfection formula developed by Dawson and Walker [44]. Based on the stub column test results, it was observed that the reduction in ultimate column capacities were ~ 9.57%, 18.24%, 31.15% and 44.00%, for perforation size ratio of 30%, 50%, 70% and 90% respectively. Further, the ultimate column capacities generated from the test were utilised to assess the compatibility of existing international design codes [39] as well as proposed design equations [9,24,40], for perforated cold-formed steel columns. Based on the comparison it was observed that most of the currently available international design equations provide conservative and reliable but scattered predictions for the design of perforated cold-formed steel SHS/RHS structural stub columns having two central circular perforations of size ratio up to 0.9.

3 Finite element modelling

3.1 Basic modelling assumptions

The experimental results reported by Singh and Singh [29] have been utilised to validate the FE modelling procedure for perforated stub columns and, further generate additional results to study the effect of key geometric parameters *viz.*, eccentricity, shapes (circular, square and hexagonal), width and depth of perforation; and cross-sectional thickness, on the buckling performance of perforated module stub columns. The numerical investigation in this paper has been conducted using the general purpose FE software ABAQUS [45]. The numerical modelling approach followed in this paper are similar to those reported in [46–49] for thin-walled structural components.

3.1.1 Geometry and boundary conditions

The measured geometric dimensions of perforated stub columns reported in Singh and Singh [29] has been utilised to develop FE models as provided in Table 1, where *B*, *D*, *t*, *L*, r_i, *w* and *d* represent the section width, section depth, thickness, overall length of stub column, inner corner radius, flat element width and diameter of perforation respectively. The definition of the symbols of geometric parameters are also detailed in Fig. 2 (a). To achieve the fixed-ended boundary conditions employed in the laboratory tests, the ends of the stub columns have been coupled with two concentric reference points – RP1 and RP2 (see Fig. 2 (b)). All the degrees of the two reference points have been restrained in all direction, except that the translational degree of freedom of RP2 along the member length has been allowed. The stub column, having two opposite circular perforation at mid-height considered herein for validation, was loaded through RP2 (see Fig. 2 (c)). The concentrated load has been applied incrementally using the modified RIKS (static) procedure available in the ABAQUS library [45]. In the RIKS procedure, load is applied proportionally considering 100 load steps and the non-linear geometric parameter has been included to capture large deformation. The method has been shown to provide sufficiently accurate results for non-linear static analysis by various researchers [46,48,50,51].

3.1.2 Material properties

The measured engineering stress-strain curves generated from the tensile coupon tests for both flat and corner regions detailed in Singh and Singh [46], have been employed in the numerical models. The key material parameters are provided in Tables 2 and 3 for flat and corner coupons respectively, in which *E*, f_y, f_u, ε_f and *n* are the Young's modulus, 0.2% proof stress, ultimate strength, percentage elongation at fracture and strain hardening exponent respectively. It may be worth noting that, a 12.5 mm and 6.0 mm width tensile coupon specimens were employed for the flat and corner coupons respectively, tested at 0.05 mm/min in the elastic range and 0.4 mm/min (beyond the elastic range) using displacement method. The non-linear stress-strain curves has been converted into true stress σ_{true} and logarithmic plastic strain $\varepsilon_{\ln}^{pl}$, as defined by the Eqs. (1) and (2) respectively, have been further employed in the FE models.

$$\sigma_{true} = \sigma_{nom}\left(1+\varepsilon_{nom}\right) \tag{1}$$

$$\varepsilon_{\ln}^{pl} = \ln\left(1+\varepsilon_{nom}\right) - \frac{\sigma_{true}}{E} \tag{2}$$

where σ_{nom} and ε_{nom} are the engineering stress and strain respectively. Poisson's ratio υ of 0.3 has been considered. As it was reported in Singh and Singh [46,47] based on the micro-hardness test, the spread of corner strength enhancement due to cold-forming was found to be concentrated within the vicinity of corner region. Hence, the flat and corner material properties are employed in the flat and corner regions, respectively. The corner strength enhancement has not been extended to the flat regions.

3.1.3 Local geometric imperfection

In order to perturb the imperfect geometry of the experimental perforated stub column into the FE model, an elastic eigenvalue analysis has been initially performed using the Lanczos Eigensolver available in the ABAQUS library [45] and the lowest buckling mode shape has been extracted. Three variations of local imperfection amplitude have been considered in the present FE modelling procedure; 1/10 and 1/100 of the cross-sectional thickness and the imperfection amplitude derived from the predictive model by Dawson and Walker [44], modified for perforated cold-formed steel by Singh and Singh [29], given by Eq. (3)

$$\omega_0 = 0.0303\left(\frac{f_y}{f_{crl}}\right)t, \tag{3}$$

where f_y is the 0.2% proof stress (presented in Table 2) and f_{crl} is the elastic critical buckling stress calculated based on the most slender plate element in the cross-section taking into account the effect of perforation. The critical elastic buckling stress can be calculated using Eqs. (4)–(6) detailed below:

$$f_{crl} = \min\left(f_{cr}, f_{cr-p}\right) \tag{4}$$

in which,

$$f_{cr} = k\frac{\pi^2 E}{12\left(1-\upsilon^2\right)}\left(\frac{t}{w}\right)^2 \tag{5}$$

$$f_{cr-p} = k_h\frac{\pi^2 E}{12\left(1-\upsilon^2\right)}\left(\frac{t}{w_h}\right)^2 \tag{6}$$

where, f_{cr} and f_{cr-p} are the critical elastic buckling stress for unperforated and perforated plate elements of the cross-section respectively; and k and k_h are the plate buckling coefficient for unperforated and perforated element (detailed in Yu and Schafer [52]) respectively. The equivalent unstiffened plate element width, w_h on either side of the perforation for circular, hexagonal and square perforations are calculated as $\left(w/2-\pi d/8\right)$, $\left(w/2-\sqrt{3}d/4\right)$ and $\left(w-d\right)/2$ respectively, as detailed in Fig. 3.

3.1.4 Finite element mesh

Because of the thin-walled nature as well as considering previous investigations [48,53], the developed FE models have been discretised using shell elements. The four-noded doubly curved shell elements with reduced integration S4R [29], having six degrees of freedoms per node has been employed in the current study. Based on mesh convergence study, an element size of ~2 times the cross-sectional thickness has been assigned to the flat regions, while in the corner regions, a finer mesh of ~6 elements have been employed to accurately simulate the curve geometry. Additionally, an element of approximately equal to the cross-sectional thickness has been used to discretised the perforation regions. A typical FE model is shown in Fig. 2 (b).

3.1.5 Validation of finite element procedure

In this section the results from the numerical simulations and those reported by Singh and Singh [29,47] are compared, particularly the load versus end-shortening curves; ultimate load; and deformed shapes. The nomenclature of cross-section followed for validation are based on those reported in Singh and Singh [29], where 60 × 40 × 2.9*d*/*w*0.9–2 represent a RHS of size 60 × 40 × 2.9 having a circular perforation of diameter d = 0.9 times the flat width w and 2 signifies a repeated test. Based on the comparison, the accuracy of the FE modelling procedure has been assessed and also verify the suitability for conducting parametric study. Table 4 presents the ratios of the experimental ultimate capacity (P_{Test}) to the numerical ultimate load (P_{FE}) for three different imperfection amplitudes. Based on the comparison, it is observed that the ultimate loads are well predicted using the imperfection amplitude predicted by Dawson and Walker [44] and t/100, whereas the predictions by using t/10 is slightly underestimated with higher coefficient of variance (COV). In addition, the complete load versus end-shortening response from the compressive test has been accurately captured by the current FE modelling procedure, including the initial stiffness, ultimate load and corresponding displacement at ultimate load and post-ultimate parts. Figs. 4 and 5 present the comparison of experimental and FE load-end shortening curves for two cross-sections namely 50 × 50 × 2.9 and 60 × 40 × 2.9 stub columns. Moreover, a comparison of the deformed mode shapes generated from the experimental and numerical results are shown in Figs. 6 and 7 for two perforated stub columns 50 × 50 × 2.9*d*/*w*0.5–1 and 60 × 40 × 2.9*d*/*w*0.9–2 respectively. It may be worth noting that, the imperfection amplitude based on Dawson and Walker [44] takes into account the effect of geometric and material properties of the cross-section; and has shown to provide suitable imperfection amplitude to accurately predict tests by several researchers [47,48,54]. Hence, the model has been employed in the parametric study detailed in this paper, to generate the local geometric imperfection amplitude for perforated module stub columns.

3.2 Material property for parametric study

In this paper, the parametric study has been conducted using the widely employed structural steel S355, considering both cold-formed and hot-rolled steel sections, having a nominal yield strength of 355 N/mm^2 and tensile strength of 470 N/mm^2 conforming to EN 10025–2 [55]. However, due to unavailability of perforated stub columns test results on S355 steels, the material properties of existing experimental results on S355 has been initially validated. Upon validation, the S355 material properties have been employed for parametric study using the FE modelling procedure for perforated stub columns detailed in Section 3.1. In the following subsections, the detail descriptions of the material model to derive stress-strain curves for both cold-formed and hot-rolled S355 steels and validation procedures have been presented.

3.2.1 Cold-formed steel

Cold-forming process induces plastic strain hardening and strength enhancement in the flat and corner regions of cold-formed steel tubular section. In the parametric study, the cold-forming effects has been considered by employing different materials in the flat and corner regions of module column. A two–stage Ramberg-Osgood material model originally developed for stainless steel [56], further modified for cold-formed steels by Gardner and Yun [35] has been adopted. In the current study, the stress-strain curves of the cold-formed structural steel S355 has been generated, considering both flat and corner regions, using the measured tensile coupon test material parameters reported by Nseir [37], as provided in Tables 5 and 6 for flat and corner material properties respectively. In the table, the cross-section RHS-S355CF-200 × 100 × 4.0 represents a RHS of size 200 × 100 × 4.0 mm made from S355 and CF for cold-formed steel

[37]. The expressions of the recommended stress (f)-strain (ε) curve for cold-formed steel developed by Gardner and Yun [35] are presented in Eqs. (7) and (8):

$$\varepsilon = \begin{cases} \frac{f}{E} + 0.002\left(\frac{f}{E}\right)^n & \text{for } f \le f_y \\ \frac{f-f_y}{E_{0.2}} + \left(\varepsilon_u - \varepsilon_{0.2} - \frac{f_u - f_y}{E_{0.2}}\right)\left(\frac{f-f_y}{f_u-f_y}\right)^m + \varepsilon_{0.2} & \text{for } f_y < f \le f_u \end{cases} \tag{7}$$

in which,

$$E_{0.2} = \frac{E}{1 + 0.002n\frac{E}{f_y}} \tag{8}$$

where ε_u, $\varepsilon_{0.2}$, and m are strain corresponding to the ultimate stress, total strain at the yield stress f_y, and strain hardening component for the curves after yield stress respectively. Further, the generated curves from the material model [35] have been compared with those measured from the tensile coupon test (detailed in Nseir [37]) as shown in Fig. 8.

3.2.2 Hot-rolled steel

In present numerical study, the structural performance of perforated module column has also been studied considering hot-rolled steel material. Yun and Gardner [36] proposed two material model for hot-rolled carbon steels based on the experimental database reported in the literature. Of the two material models, the bilinear plus non-linear hardening model has been adopted to generate stress-strain curves of S355 hot-rolled steel. The expressions of the stress-strain material model are presented in Eqs. (9)–(11). In the current study, the material properties for S355 hot-rolled steels measured from the tensile coupon test reported by Liew [38], provided in Table 7 has been employed. In the table, the identification convention ‘41T’ represents average of tensile coupon test results cut from member number 1 having cross-sectional thickness of 4 mm and section size of 120 × 80 mm [38]. The cross-section is made from S355 hot-rolled steel. The comparison of the predicted and measured stress-strain curve (detailed in Liew [38]) is presented in Fig. 9.

$$
f = \begin{cases} E\varepsilon & \text{for } \varepsilon \le \varepsilon_y \\ f_y & \text{for } \varepsilon_y < \varepsilon \le \varepsilon_{sh} \\ f_y + \left(f_u - f_y\right)\left\{0.4\left(\frac{\varepsilon-\varepsilon_{sh}}{\varepsilon_u-\varepsilon_{sh}}\right) + 2\left(\frac{\varepsilon-\varepsilon_{sh}}{\varepsilon_u-\varepsilon_{sh}}\right) / \left[1+400\left(\frac{\varepsilon-\varepsilon_{sh}}{\varepsilon_u-\varepsilon_{sh}}\right)^5\right]^{1/5}\right\} & \text{for } \varepsilon_{sh} < \varepsilon \le \varepsilon_u \end{cases} \quad (9)
$$

in which,

$$
\varepsilon_u = 0.6\left(1-\frac{f_y}{f_u}\right) \quad \text{but } \varepsilon_u \ge 0.06 \text{ for hot-rolled steels} \quad (10)
$$

$$
\varepsilon_{sh} = 0.1\frac{f_y}{f_u} - 0.055 \quad \text{but } 0.015 \le \varepsilon_u \le 0.03 \quad (11)
$$

3.2.3 Validation of material property

In this section, the accuracy of the predicted stress-strain curves derived using the material models recommended by Gardner and his co-worker [35,36], has been assessed. Experimental investigations on S355 (SHS and RHS) stub columns, conducted by Nseir [37] and Liew [38] for cold-formed and hot-rolled steel respectively, has been utilised. The measured geometric dimensions of cold-formed and hot-rolled steel stub columns are provided in Tables 8 and 9, respectively. In Table 9, the cross-section ID '1ST4' represents the stub column from member 1 having wall thickness of 4 mm and cross-section size of 120 × 80 mm [38]. The numerical modelling protocols detailed in Section 3.1 has been employed to initially developed FE models. The flat and corner material curves generated using material model detailed in Section 3.2.1, has been utilised to the flat and corner regions of the FE model for cold-formed steel stub columns, while the stress-strain curve generated using the material model provided in Section 3.2.2 has been employed in both the flat and corner regions for hot-rolled steel stub columns. Three variations of the local geometric imperfection amplitude have been adopted in the non-linear analysis, namely 1/10 and 1/100 of the cross-sectional thickness and the imperfection amplitude from the predicted model [54] given by Eq. (12). Further, the results from the numerical simulations and experimental results [37,38] are compared and the accurateness of the material models has been examined, utilizing the three imperfection amplitudes.

$$
\omega_0 = 0.023\left(\frac{f_y}{f_{crl}}\right)t \quad (12)
$$

Tables 10 and 11 present the ratios of the experimental to the numerical ultimate load for varying geometric imperfections, for cold-formed and hot-rolled steel stub columns, respectively. It can be observed that the ultimate loads are generally well-predicted for imperfection amplitude of 1/10 of the cross-sectional thickness for cold-formed steel, while imperfection amplitude values of 1/100 of the cross-sectional thickness and prediction model [54] for hot-rolled steels. Moreover, the load versus end shortening curves generated from the numerical models and those reported by Nseir [37] and Liew [38] for cold-formed steel and hot-rolled steel respectively, are compared in Figs. 10 and 11. Overall, good agreement between the test results and those generated from the numerical models have been achieved, except the lateral shift in the load-end shortening curve for cold-formed steel stub columns (similar deformation pattern). Similar deviation in the load-end shortening curves generated from the FE models against the test results was reported by Nseir [37]. This may be related to the lack of correction in the end-shortening data generated from linear variable displacement transducers (LVDTs) reported by Nseir [37]. Hence, it may be concluded that, the stress-strain curves generated using material models [35,36] can represent the measured stress-strain curve and also predict the ultimate column capacity accurately, and therefore, the material models [35,36] (for both cold-formed and hot-rolled material) have been employed for parametric study in this paper. It may be worth mentioning that, several attempts were reported in the literatures [57–59] to quantify the magnitude and distribution of residual stress induced in the structural member during cold-forming, welding etc. However, it has been reported that the effect of residual stress on the ultimate load capacity and load-end shortening behaviour are not significant [60–62], and hence residual stresses are not included in the current FE modelling procedure.

4 Parametric study

4.1 General

In the paper, the critical buckling performance of stub column having a perforation on one side of the cross-section has been investigated. A typical geometry of the stub column is shown in Fig. 12 (a). The cross-sectional dimension of the perforated (PSHS) and unperforated square hollow section (USHS) stub column adopted herein has an outer dimension of 200 mm. The length of the stub columns has been set equal to four times the cross-sectional size (4 × 200 mm = 800 mm), which is based on the guidelines presented in [63] for stub column test, where the length of the compression member (L) should be ≤20 times the least radius of gyration of the cross-section. However, the length of the column should be greater than or equal to three times the width of the widest plate element to avoid end effects. The FE modelling procedure in the parametric study are similar to those detailed in Section 3.1, except that the stress-strain curves generated from the material model [35,36] for S355 cold-formed and hot-rolled material has been adopted. Further, a single perforation is made on one side of the SHS. Typical FE model and the boundary conditions considered for parametric study is shown in Figs. 12 (b) and (c) respectively. The distance '*e'* of the location of perforation has been measured from the bottom of the column (unloaded end) to the centre of the perforation. The effect of eccentricity (e/L) of perforation has been studied by varying the value of e/L ranging from 0.1 to 0.5. In addition, the effect of perforation width has been investigated by varying the perforation size ratio (d/w) from unperforated to 0.9. Besides, the effect of perforation shapes has been examined by considering three commonly used perforations namely circular, square, and hexagonal shape. Moreover, reduction in the critical buckling load due to perforation height (h) has been explored by increasing the height to diameter ratio (h/d) from 1.0 to 2.5. Further, the effect of cross-sectional thickness on the critical buckling capacity of perforated module column has been investigated by varying the cross-sectional thickness from 5.0 mm to 10.5 mm, covering all the cross-sectional classification under pure compression from Class 1–3 to Class 4 detailed in EN 1993–1-1 [64].

5 Analysis of results and design recommendations

In this section, a systematic study on the effect of various parameters on the ultimate capacity of stub column has been discussed. In the first part of the discussion, the effect of eccentricity on the critical buckling strength has been presented. Upon determination of the critical location of perforation (e/L) from the first part, the effect of width, shape, and height of perforations has been further investigated in the consecutive part of the study. Furthermore, FE models have been made to investigate the effect of cross-sectional thickness on the critical buckling strength of perforated stub column considering the critical eccentricity (e/L). It may be mentioned that the cross-sectional thickness adopted in the present study are in such a way that all the section classification under pure compression from, Class 1–3 to Class 4, has been covered based on the EN 1993-1-1 [64]. Finally, the applicability and accurateness of the currently available design equations for perforated steel compression member detailed in AISI S100-16 [39] and those proposed by researchers [9,24,25,40,41] has been assessed, through reliability analysis, for design of cold-formed and hot-rolled steel stub module columns having single perforation.

5.1 Deformed shapes

Fig. 13 (a)–(j) show typical deformed shapes of USHS (Fig. 13 (a) and (b)) and PSHS (Fig. 13 (c)–(j)) stub columns superimposed with stress contour (i.e. Von-Mises stress) at ultimate (deformation, $\delta = \delta_u$) and post-ultimate column capacity (deformation, $\delta = 1.5\delta_u$) for t = 8.5 mm (i.e., Class 1–3 cross-section). For comparison purpose, stub column having a circular perforation of d/w = 0.3 located at e/L =0.2 (Fig. 13 (c) and (d)) and a set of three stub columns (Fig. 13 (e)–(j)), having circular, hexagonal and square perforations of d/w = 0.7 located at e/L = 0.5 have been considered. Areas having stress value ≥ yield stress (i.e. f_y = 492.14 MPa for cold-formed steel), are grey-coloured. It can be seen from Fig. 13 (a) that, at ultimate load ($\delta = \delta_u$) for the unperforated stub column, most of the column regions are uniformly stressed, indicating that the regions are fully effective; however, for perforated stub columns, as shown in Figs. 13 (c), (e), (g) and (i), the stress distribution is altered due to the introduction of perforation. For the perforated stub column with smaller perforation size of d/w = 0.3 (Fig. 13 (c)), most part of the column is uniformly stressed (similar to that of unperforated column), except in the perforated plate element in which the areas near perforation and upper region (near the end) are yielded and local buckling is initiated near the perforation. On the other hand, for the perforated stub column with larger perforation (i.e. d/w = 0.7) as shown in Fig. 13 (e), (g) and (i), the areas near the perforation regions, i.e. on either sides of perforation (left and right) seemed to be yielded, and initiation of local buckling is observed. Additionally, it is also observed (from Fig. 13 (e), (g) and (i)) that some parts of unperforated plates (located around 90 degrees adjacent to perforated plate) and most parts of the unperforated plate (opposite to perforated plate) are found to be yielded, indicating that these regions are fully effective in resisting the axial load. Further, at post ultimate load (i.e., deformation, $\delta = 1.5\delta_u$), local buckling can be seen to have occurred at column mid-height for the unperforated stub column and at the perforation location in the case of the perorated stub column. Hence, it may be concluded that the size and location of perforation can influence the initiation of local buckling for a perforated stub column. Besides, it is witnessed that, for stub column having similar perforation size and location, the stress distribution and deformed shapes are found to be similar as shown in Fig. 13 (e)–(j). Furthermore, the areas which are located above and below the perforation are less effective in taking axial load (as indicated by minimal stress at both ultimate and post-ultimate load). Thus, it is apparent that the region on either side of perforation (i.e.

towards the left and right sides) are more effective than those which lie above and below the perforation. Hence, stub columns having similar perforation width may have equivalent column capacity. Additionally, Fig. 14 (a)–(d) present the comparison of typical deformed shapes (along with Von-Mises stress contour) of cold-formed and hot-rolled steel module columns. It may be observed that, although the stress distribution patterns are slightly different which may be due to difference in yield stresses (average 0.2% proof stress for cold-formed steel, f_y = 492.14 MPa > yield stress of hot-rolled steel, f_y = 411.63 MPa), overall deformed shapes are similar at both ultimate and post-ultimate load. Hence, it is apparent that both the steel materials may exhibit similar buckling capacity.

5.2 Variation of ultimate column capacity

5.2.1 Effect of eccentricity

In this section, the effect of position or location of single circular perforation on the local buckling performance of stub module column has been investigated. Figs. 15 and 16 show the variation of normalised load $P / A_g f_y$ (where A_g = gross-cross-sectional area) versus end-shortening curves for different values of eccentricity ranging from $0.1 \le e/L \le 0.5$ considering d/w = 0.5 and Class 1–3 cross-section ($c/t\varepsilon$ = 28.73 < 42 for cold-formed steel and $c/t\varepsilon$ = 25.11 < 42 for hot-rolled steel, where is the flat element width and $\varepsilon = \sqrt{\left(235 / f_y\right)\left(E / 210000\right)}$ detailed in Eurocode 3 [64]). It is observed from Fig. 15 that the critical buckling load P_u increases with decreasing value of eccentricity (i.e., as the perforation is close to unloaded-end of the stub column) for cold-formed steel. On the other hand, the effect of eccentricity on the ultimate column capacity is less significant (as compare to cold-formed steel) for perforated hot-rolled steel column as can be seen in Fig. 16. Besides having similar cross-sectional dimensions, it may be noticed from Figs. 15 and 16 that, the normalised load versus end-shortening curves for cold-formed steel stub columns reach the yield load ($A_g f_y$), which may be due to the strain hardening effect (resulted from cold-forming) as compared to hot-rolled steel stub columns. Additionally, the effect of eccentricity on the ultimate column capacity for various d/w has been studied in detailed. Typical variations of the normalised ultimate load P_u / P_0, where P_u and P_0 are the ultimate load of perforated and unperforated (solid or non-perforated of similar cross-sectional dimensions), against e/L for various range of perforation size ratio d / w ranging from 0.1 to 0.9, has been plotted in Fig. 17 and 18 for cold-formed and hot-rolled steel respectively, considering stub module column of thickness t = 8.5 mm (Class

1–3). It can be seen that, the reductions in cold-formed steel module columns are found to be more prominent as compared to those of hot-rolled steel columns for which the reduction is very less or almost no reduction, this may be related to enhanced strain hardening behaviour generally exhibited by cold-formed steels (generated from cold-working) as compared to hot-rolled steels for which there is less or no strain hardening effect. Further, the rate of reduction in buckling load is steeper as the perforation size increases and the steepest being largest perforation size ratio, i.e., d/w = 0.9, as clearly observed in cold-formed steel stub columns. The percentage reduction in critical buckling strength for cold-formed steel are found to be ~0.44%, 2.46%, 3.16%, 3.33% and 4.77% for d/w = 0.1, 0.3, 0.5, 0.7 and 0.9 respectively as the eccentricity of the perforation, e/L increases from 0.1 to 0.5, whereas the reductions in those of the hot-rolled steel columns for d/w = 0.1, 0.3, 0.5, 0.7 and 0.9 are respectively estimated to be ~0.33%, 0.28%, 0.82%, 0.77% and 1.42%. Further, based on the Figs. 15–18, it is observed that the reduction in the ultimate load is maximum when the perforation is located at e/L = 0.5. Thus, it can be concluded that the reduction in critical buckling load of perforated module column is maximum when the perforation is located mid-height of module stub column.

5.2.2 Effect of perforation shape

As mentioned in Section 1, perforations of different shapes and dimensions, depending on their purposes and needs, may be provided on a structural module column and thus, the introduction of perforation will alter the stress distribution as observed in Section 5.1. In this Section, the effect of perforation shapes on the critical buckling performance of perforated module columns is investigated by considering three commonly use perforation shapes namely circular, hexagonal, and square shapes. For comparison purpose, the perforation width (d) and height (h) of perforation has been kept constant except for hexagonal perforation, for which the depth is ~1.1547 times the diameter of perforation. Additionally, a hexagonal perforation shape of equal height (EH) has also been considered, by reducing the depth of perforation. Fig. 19 presents typical perforation shapes considered for parametric study. Typical variations of normalised critical buckling strength, P_u / P_0 against the eccentricity of perforation e/L for different perforation shapes both for cold-formed and hot-rolled steel module columns is provided in Fig. 20, considering d/w = 0.7 and Class 1–3 cross-sectional thickness, t = 8.5 mm (i.e., $c/t\varepsilon$ = 28.73 < 42 for cold-formed steel and $c/t\varepsilon$ = 25.11 < 42 for hot-rolled steel). In the figure, ‘CF’ and ‘HR’ represent cold-formed and hot-rolled steel material. As it can be seen from Fig. 20 that, despite the descending order of column capacities of perforated stub columns having circular, hexagonal and square perforation shapes are generally observed to be in the order: circular > hexagon > square, perforation shapes have marginal effect on the critical buckling capacity of module column. This may be related to the fact that, although the stub columns have different shapes, the stress distribution is similar as observed in Section 5.1. Additionally, for the two hexagonal shapes considered of different depths, the reduction in buckling performance is similar and no significant difference is seen. In the following section, the effect of perforation height will be discussed in detailed.

5.2.3 Effect of perforation width

The effect of perforation size (width or diameter of perforation) on the critical buckling strength of perforated module column is investigated in this section. Figs. 21 and 22 show the variation of P_u / P_0 against d / w for various eccentricities ranging from 0.1 to 0.5, for cold-formed and hot-rolled steel respectively, considering a Class 1–3 cross-section of thickness 8.5 mm with a circular perforation. From Fig. 21, it can be seen that, the buckling strength of cold-formed steel module column decreases in a nearly linear behaviour with increasing d/w for all values of eccentricities considered (e/L = 0.1, 0.2, 0.3, 0.4 and 0.5), and also, the reduction is found to be eminent when the perforation is located at column mid-height. However, the effect of eccentricity on P_u / P_0 for hot-rolled steel is found to be insignificant (as can be seen in Fig. 22), although P_u / P_0 decreases linearly with increasing d/w. A similar observation has been seen in the section 5.2.1. In addition, the effect of d/w is studied considering two different cross-sections, namely Class 1–3 ($c/t\varepsilon$ < 42.0) and Class 4 ($c/t\varepsilon$ > 42.0). Figs. 23 and 24 present typical plots of P_u / P_0 against d/w for Class 1–3 and Class 4 cross-sections based on Eurocode 3 [64], considering three perforation shapes (viz, circular, square and hexagonal shapes). It is observed from Fig 23, that for $d/w \leq 0.1$, the reduction in the critical buckling capacity both for cold-formed steel and hot-rolled steel are negligible for Class 1–3 cross-sections. However, for larger perforation of $d/w > 0.1$, a nearly linear reduction in $\left(P_u / P_0\right)$ with increasing d/w both for cold-formed and hot-rolled steel is observed. The maximum reduction in normalised ultimate buckling load $\left(P_u / P_0\right)$ for cold-formed and hot-rolled steel module stub columns when d/w = 0.9 are ~75% and 79% respectively. Furthermore, as seen in Fig. 24, the reductions in critical buckling strength of cold-formed steel module columns for Class 4 cross-sections are found to be negligible for perforation size ratio, d/w up to 0.3, but reduced gradually in a mild nonlinear trend with increasing d/w. However, in the case of hot-rolled steel, the reduction in column strength is found to be increasing as d/w increases, following similar trend as that of cold-formed steel for $d/w > 0.3$. The percentage reduction in P_u / P_0 at $d/w = 0.9$ for Class 4 cross-sections are respectively predicted as ~78% and 74% for cold-formed and hot-rolled steel module columns. It may also be witnessed from Figs. 23 and 24 that, the buckling capacities of perforated module columns with circular perforation are generally found to be higher as compared to square and hexagonal shape perforations, although the differences in the buckling strength are in the range of ~ ±1.0%. It may be due to similar perforation width which has dominant effect as compared to the load transfer through the edges of the perforation as observed in Section 5.1.

Also, in this section the performances of cold-formed and hot-rolled steel module stub columns have been compared. The ultimate column capacities generated from the FE normalised with yield load ($A_g f_y$) are plotted against d/w for both Class 1–3 and Class 4 cross-sections, as shown in Figs. 25 and 26 respectively. It can be seen from the figures that, for similar cross-sectional size (200 × 200 mm) and thickness (8.5 mm), cold-formed steel perforated stub columns provide higher normalised ultimate column capacities ($P_u / A_g f_y$) as compared to those of hot-rolled steels, both for Class 1–3 and Class 4 cross-sections. Additionally, the cross-sectional performance for cold-formed steel columns are found to more prominent for Class 1–3 cross-section with lower values of d/w as compared to Class 4 cross-section. However, as d/w increases, the column capacities of perforated cold-formed steel columns are close to those of hot-rolled steel columns. On the other hand, the behaviour of cold-formed and hot-rolled steels stub columns are observed to be similar for $d/w \geq 0.3$. On an average, as the perforation size ratio ranges from 0.1 to 0.9, the performance of perforated cold-formed steel stub columns is 7% and 2% higher than those of hot-rolled steel columns, respectively for Class 1–3 and Class 4 cross-sections. It may be worth mentioning that, the increase in cross-sectional performance generally observed in perforated cold-formed steel stub columns may be related to strain hardening effect induced from cold-working and thus, recommended for use in modular steel construction.

The behaviour of load versus end-shortening curves of different values of d/w (ranging from 0.1 to 0.9) has been studied in this section. Typical variations of normalised buckling load $\left(P / A_g f_y\right)$ versus end-shortening curves for Class 4 cold-formed and hot-rolled steel cross-sections are shown in Figs. 27 and 28 respectively, whereas for those Class 1–3, the curves (load-displacement) are shown in Figs. 29 and 30 for cold-formed and hot-rolled steel sections, respectively. Based on the predicted FE results, it is observed that the elastic stiffness and critical buckling stress $\left(P_u / A_g f_y\right)$ increases with decreasing value of *d*/*w*. Besides, from Figs. 27–30, it can be witnessed that the load-end shortening curves generated from cold-formed steel module columns offer a more rounded curves as compared to those of hot-rolled steel columns. Again from Figs. 29 and 30, it can be seen that for $d/w \geq 0.5$, the ultimate loads of cold-formed steel stub columns are predicted to be larger than the yield stress $\left(A_g f_y\right)$, whereas for hot-rolled steel stub column, ultimate loads are higher than yield stress for $d/w \geq 0.3$, indicating the effect of strain hardening.

5.2.4 Effect of perforation height

This section discusses the effect of perforation height (or depth of perforation) on the buckling strength of perforated module column. Typical perforation shapes *viz*., elongated circular (flat-oval) and hexagonal; and rectangular, considered for the present study are shown in Fig. 31, where the height (*h*) of perforation is two times the width of perforation, i.e., $h/d = 2.0$. In the present study, the height of perforation is varied from 1.0 to 2.5 times the width of perforation, keeping $d/w = 0.7$ as constant. The Typical variation of normalised critical buckling stress $P_u / P_{1.0}$, in which where $P_{1.0}$ is the critical buckling capacity when the perforation height to width ratio is 1.0 (i.e., $h/d = 1.0$), against perforation depth to height ratio (*h*/*d*) for cold-formed and hot-rolled steels are respectively shown in Fig. 32 and 33. Based on the figures, it is observed that the reduction in critical buckling capacities of the perforated module columns are in the range of ~ ± 1.0%, i.e., negligible with increasing perforation depth for the three perforation shapes considered, both for cold-formed and hot-rolled steel module columns. This may be due to the fact that, the increase in perforation height does not affect the overall effective width of the cross-section at the perforation location, as shown in Fig. 34. Thus, it is apparent that load carrying of stub column having different perforation height will be equivalent. Hence, it can be concluded that perforation width has major influence on the critical buckling performance of module stub column having single perforation at mid-height of the column, as compared to perforation depth, for which the reduction is negligible.

5.2.5 Effect of thickness

The effect of cross-sectional thickness on the critical buckling axial load of perforated module column is presented in this section. The sectional thickness of the SHS of size 200 × 200 having a single circular perforation at critical location, i.e., $e/L = 0.5$, has been varied from 5.5 mm

($c/t\varepsilon$ = 47.60 for cold-formed steel) and 5.0 mm ($c/t\varepsilon$ = 46,28 for hot-rolled steel) to 10.5 mm ($c/t\varepsilon$ = 22.13 for cold-formed steel and $c/t\varepsilon$ = 19.35 for hot-rolled steel) so that all the section classification (i.e., Class 1–4) based on EN 1993–1-1 [64], has been covered in the present study. Typical variation of P/A_gf_y versus end-shortening curves for various values of t, considering smaller perforation size of d/w = 0.3 located at e/L = 0.5 are shown in Figs. 35 and 36 for cold-formed and hot-rolled steel stub columns respectively, while for larger d/w = 0.9 the normalised load-displacement curves for cold-formed and hot-rolled steel columns are respectively shown in Figs. 37 and 38. It is observed from the Figs. 35–38 that P_u/A_gf_y and displacements at ultimate load, δ_u increases with increasing value of t. Again, it is witnessed that the load-displacement curves with d/w = 0.3 are relatively flatter for higher t, which may be related to strain hardening effect and the ultimate load of the perforated module columns are found to be larger than the yield load (A_gf_y) except for the Class 4 cross-section (t = 5.5 mm), for which the occurrence of local buckling hinders reaching yield load. On the other hand, for larger perforation size of d/w = 0.9, a certain degree of strain hardening has been observed for relatively thick section as can be seen in Figs. 37 and 38, and the ultimate load of the perforated columns are found to be lesser than the yield stress which may be due to smaller cross-sectional size resulted from large circular cut-outs on one side of the cross-sections. In addition, the load-end shortening curves generated from the cold-formed steel module column induce a distinctly rounded and pronounce strain hardening effect as seen in Figs. 35 and 37 when compared to those of hot-rolled steel columns as presented in Figs. 36 and 38.

Further, the variation of P_u / P_0 with d/w for different thickness ranging from t = 5.5 mm for cold-formed and 5.0 mm for hot-rolled to 10.5 mm are presented in Figs. 39 and 40 for cold-formed and hot-rolled steel respectively. From Fig. 39, it can be seen that, for all the thickness investigated for cold-formed steel stub columns, the ratio of ultimate buckling strength of perforated to the corresponding unperforated (solid) stub column P_u / P_0 decreases with increase in perforation diameter for $d/w \leq 0.3$, except for t = 5.5 mm and 6.5 mm, for which the reductions are negligible. However, for higher perforation size ratio, $d/w > 0.3$ the predicted P_u / P_0 are similar for all the thickness analysed, except for Class 4 cross-section (t = 5.5 mm) for which the reduction is relatively higher and it may be due to lesser effective area as compared to thick sections. Whereas, unlike cold-formed steel columns, the reduction in critical buckling capacity for hot-rolled steel columns are similar for $t \geq 6.5$ mm and for t < 6.5 mm, P_u / P_0 is slightly decreasing as d/w increases, as presented in Fig. 40.

5.3 Assessment of codified design rules for perforated steel members

5.3.1 General

In this section, the applicability of the developed design equation for perforated steel structural member presented in AISI S100-16 [39] and those proposed by researchers [9,24,25,40,41] has been assessed for design of cold-formed and hot-rolled steel stub module columns having single perforation at mid-height of the column. In calculation the unfactored design strengths, the effective length of the stub columns has been taken as half of the member length (i.e., 0.5 *L*) for fixed-ended boundary conditions. Hence, the effective length factor (*K*) of the stub column is considered as 0.5. Further, the design strength of the stub columns has been calculated based on the nominal cross-sectional dimensions and weighted average measured material properties for cold-formed and hot-rolled steels, respectively reported by Nseir [37] and Liew [38]. It may be worth mentioning that most of the current design equations for perforated compression members are presented for perforation size ratio up to a maximum of 0.7.

5.3.2 Design formulae in the AISI design standard

In Chapter E of American Iron and Steel Institute, AISI Standard [39], design formulae are provided to estimate the ultimate capacity of structural members under axial compressions. Based on the Chapter, the nominal axial capacity of a compression member shall be the minimum of the following instabilities – yielding and global buckling (flexural) $\left(P_{ne}\right)$, local buckling interacting with yielding and global buckling $\left(P_{nl}\right)$ and distortional buckling $\left(P_{nd}\right)$. In the present study, because of the closed section nature, distortional buckling may not occur and hence be ignored. Additionally, since the columns are considered short enough to avoid flexural buckling, the predicted P_{ne} are found to be larger than nominal axial strength for local buckling $\left(P_{nl}\right)$. According to Section E3 of AISI design code, the nominal axial strength for local buckling (interacting with yielding and global buckling) shall be estimated either by Effective Width Method (EWM) and Direct Strength Method (DSM).

5.3.2.1 Local buckling based on Effective Width Method

Based on section E3.1 of AISI Standard [39], the nominal axial strength P_{nl-EWM} for local buckling based on the Effective Width Method is calculated as follows:

$$P_{nl-EWM} = A_e F_n \leq P_{ne} \tag{13}$$

in which,

F_n = Global column stress,

A_e = Effective area calculated at stress F_n, and

P_{ne} = Nominal strength considering yielding and global buckling.

The effective width of flat elements of the cross-section is estimated based on Appendix 1 of AISI Standard [39]. For perforated stiffened elements of $0 \leq d/w \leq 0.5$ and $w/t \leq 70$, the effective width is calculated based on Eq. (14) as follows:

$$\begin{aligned} &\text{For } \lambda \leq 0.673, \quad b = (w - d) \\ &\text{For } \lambda > 0.673, \quad b = \frac{w}{\lambda}\left\{1 - \frac{0.22}{\lambda} - \frac{(0.8d)}{w} + \frac{(0.085d)}{w\lambda}\right\} \end{aligned} \tag{14}$$

in which,

$\lambda = \sqrt{F_n / f_{crl}}$;

5.3.2.2 Local buckling based on Direct Strength Method

The nominal axial capacity for local buckling ($P_{nl\text{-}DSM}$) based on Direct Strength Method of [39] is from the modifications proposed by Moen and Schafer [65] for design of cold-formed steel columns with perforations and estimated from formulae given in Eq. (15) as follows:

$$\begin{aligned} &\text{For } \lambda_l \leq 0.776; \quad P_{nl-DSM} = P_{ne} \leq P_{ynet}, \\ &\text{For } \lambda_l > 0.776; \quad P_{nl-DSM} = \left\{1 - 0.15\left(\frac{P_{crl}}{P_{ne}}\right)^{0.4}\right\}\left(\frac{P_{crl}}{P_{ne}}\right)^{0.4} P_{ne} \leq P_{ynet}, \end{aligned} \tag{15}$$

in which,

$\lambda_l = \sqrt{P_{ne} / P_{crl}}$;

$P_{ynet} = A_{net} f_y$;

$A_{net} = A_g - A_p$; where,

$$P_{crl} = A_g f_{crl},$$
$$A_p = d * t.$$

Based on Section 2.3.2.2 of Appendix 2 of AISI Standard [39], the local buckling stress, f_{crl} for element with perforation is estimated considering both for unstiffened elements at the perforation location and as a separate element where perforation is not located. For element at the perforation location, the stress has been multiplied by a ratio of A_{net}/A_g, to account for the effect of net cross-sectional area.

5.3.3 *Design equation proposed by Miller and Peköz*

A simplified formula for the treatment of plate having any shape of perforation was developed by Miller and Peköz [40]. Based on the formulae, the effective width *b* can be determined as follows:

$$\begin{aligned} &\text{if } w - b_{DW} \geq d \text{ then } b = b_{DW} \\ &\text{if } w - b_{DW} < d \text{ then } b = w - d \end{aligned} \tag{16}$$

where b_{DW} is the effective design width. Expressions are provided in many design codes to estimate the effective design width, b_{Dw} for an unperforated plate under uniform compressions as follows:

5.3.3.1 *Effective design width based on European, American, and Australian standards*

The European code EC3-1-5 [66], North American specification AISI S100-16 [39] and Australian/New Zealand standard AS/NZ 4600 [67] provide guidelines for determination of effective cross-sectional width of an internal flat compression element, as presented in Eq. (17) as follows:

$$\begin{aligned} &\text{For } \bar{\lambda}_p \leq 0.673; \quad b_{DW} = w \\ &\text{For } \bar{\lambda}_p > 0.673; \quad b_{DW} = w\left(\frac{1 - 0.22/\bar{\lambda}_p}{\bar{\lambda}_p}\right) \leq w \end{aligned} \tag{17}$$

where $\bar{\lambda}_p = \sqrt{f_y / f_{cr}}$. The column capacity based on Miller and Peköz [40] simplified formula using the above effective design equation is represented by $P_{MP\text{-}EC3}$.

5.3.3.2 *Effective design width based on British standard*

The British standard, BS-5950-5 [68] provides guidelines to estimate the effective design width as follows:

For $f_y / f_{cr} \leq 0.123$, $\quad b_{DW} = w,$

For $f_y / f_{cr} > 0.123$, $\quad b_{DW} = w\left[1+14\left\{\left(\frac{f_y}{f_{cr}}\right)^{1/2} - 0.35\right\}^4\right]^{-0.2}$ (18)

The column capacities by Miller and Peköz [40] simplified formula using the above effective design equation is represented by $P_{MP\text{-}BS}$.

5.3.4 Design formulae developed by Abdel-Rahman and Sivakumaran

Abdel-Rahman and Sivakumaran [41] developed a FE model to study the ultimate capacity of perforated lipped channel short columns. The parametric study covered various geometric parameters, including flat element width to thickness ratio w/t (ranging from 31.3 to 194.2), perforation width to flat element width ratio d/w (≤ 0.6), and perforation height to perforation width ratio h/d (ranging from 1.0 to 3.0). The design formulae to estimate effective width b of a stiffened plate element of width w having a perforation of size d and subjected to uniformed compressive load, proposed by Abdel-Rahman and Sivakumaran [41] is presented in Eq. (19) as follows:

$$b = 0.95t\left(\frac{kE}{F_{\max}}\right)^{1/2}\left[1-0.208\frac{t}{w}\left(\frac{kE}{F_{\max}}\right)^{1/2} - 0.58\frac{d}{w}\right] \leq w-d \qquad (19)$$

where k and $F_{\max}$ are the plate buckling coefficient and maximum design stress; and the last term $\left(0.58\frac{d}{w}\right)$ of Eq. (19) represents the effect of perforation on the effective width of the perforated plate. The column capacity based on effective width equations proposed by Abdel-Rahman and Sivakumaran [41] is represented by P_{ARS}.

5.3.5 Design formulae developed by Shanmugam et al.

Shanmugam et al. [9] conducted an extensive numerical study to investigate the post-buckling behaviour and the ultimate load capacity of perforated plates considering various critical parameters such as plate slenderness, opening size, boundary conditions and nature of loading. The study covered plate slenderness *w/t* varied from 20 to 70 while perforation size ratio up to 0.7 ($d/w \leq 0.7$) was examined. Further, using the generated plate capacities, a design formula to estimate the ultimate load carrying capacity $\left(P_{STT}\right)$ of axially compressed perforated plates was developed through the best-fit regression analysis and presented as follows:

$$\frac{P_{STT}}{P_{sq}} = k_1\left[\frac{A_0}{A_s}\right] + k_2\left[\frac{A_0}{A_s}\right]^{1/2} + k_3 \tag{20}$$

For $0 < d/w < 0.4$,

$k_1 = -4m^2 + 1.58m - 0.1286;$

$k_2 = 3m^2 - 1.52m - 0.8674;$

$k_3 = -m^2 + 0.49m + 0.9585.$

For $0.4 < d/w < 0.7$

$k_1 = 0;$

$k_2 = -0.96;$

$k_3 = 0.973.$

in which,

A_0 = Total surface area of perforations;

A_s = Total surface area of the member;

$m = \left(w/t\right)/100$

where k_1, k_2 and k_3 are different sets of coefficients and P_{sq} is the squash load.

5.3.6 Design formulae proposed by Dhanalakshmi and Shanmugam

Experimental and numerical investigations to study the behaviour of cold-formed equal-angle stub columns subjected to axial or eccentric loading was conducted by Dhanalakshmi and Shanmugam [25]. Key geometric parameters such as plate slenderness ratio ranging from 20 to 60, perforation shapes and size ratio ($d/w \leq 0.6$) and number of perforations were considered. Further, a simplified design equation to predict the ultimate strength $\left(P_{DS}\right)$ of perforated equal-angle stub columns was developed by Dhanalakshmi and Shanmugam [25] using the data obtained from the parametric study as follows:

$$\frac{P_{DS}}{P_{sq}} = k_1\left(\frac{A_0}{A_s}\right) + k_2\left(\frac{A_0}{A_s}\right)^{1/2} + k_3; \tag{21}$$

in which,

A_0 = Surface area of perforations.

A_s = Total surface area of the member

$k_1 = -4.5579m^2 + 4.4862m - 1.3724;$

$k_2 = -0.8107m^2 + 1.0577m - 0.3354;$

$k_3 = 2.5357m^2 - 2.8364m + 1.0908;$

where k_1, k_2 and k_3 are different sets of coefficients and P_{sq} is the squash load.

5.3.7 Design formulae proposed by Shanmugam and Dhanalakshmi

A simplified design equation was developed by Shanmugam and Dhanalakshmi [24], for design of perforated plain and lipped channel sections stub columns containing perforations of all kinds of shapes. The study was conducted using validated numerical models, considering wide range of geometric parameters such as web plate slenderness ranging from 29.3 to 133.7 and perforation size ratio, $d/w \leq 0.6$. The two basic parameters used to derive the design equation are namely – the web plate slenderness ratio (w/t) and perforation area ratio (A_0/A_S). The design equation developed by Shanmugam and Dhanalakshmi [24] to estimate the ultimate load (P_{SD}) of perforated channel stub columns having either single or multiple perforation of circular, square and manufacturer's opening shapes is presented in Eq. (22) as follows:

$$\frac{P_{SD}}{P_{sq}} = k_1\left[\frac{A_0}{A_s}\right] + k_2\left[\frac{A_0}{A_s}\right]^{1/2} + k_3 \tag{22}$$

in which,

A_0 = Total surface area of perforations.

A_s = Total surface area of the stub column

$k_1 = 1.185m^3 - 3.8487m^2 + 3.7321m - 1.2336;$

$k_2 = 0.1111m^2 + 0.0932m - 0.7763;$

$k_3 = 0.11m^2 - 0.5681m + 1.1412;$

$$m = (w/t)/100$$

where k_1, k_2 and k_3 are different sets of coefficients and P_{sq} is the squash load.

5.4 Reliability analysis

Reliability analysis has been carried out in order to assess the applicability of the developed design equation for perforated steel structural member presented in AISI S100-16 [39] and those proposed by researchers [9,24,25,40,41] for the design of single perforated cold-formed and hot-rolled steel stub module columns. The analysis has been carried considering the procedures outlined in Section B of AISI specification commentary [69]. The statistical parameters such as mean P_m and coefficient of variance V_p from the comparison of FE column capacities and design prediction ratios (detailed in Tables 12 and 13). The resistance factor of (ϕ) of 0.85 has been used for direct strength method [39] based on AISI specification [69]. In addition, for the purpose of direct comparison, ϕ = 0.85 has been adopted for all proposed design equations [9,24,25,40,41], following similar approach to Refs. [62,70]. The dead load (DL) to live load (LL) ratio of 1/5 and 1/3 respectively for cold-formed and hot-rolled steels, are considered as recommended by AISI specification [69] and AISC 360 [71]. The mean value of material (M_m) and fabrication factor (F_m) of 1.10 and 1.00 and their corresponding coefficient of variance (V_M) and (V_F) of 0.10 and 0.05 respectively, has been adopted for cold-formed steel as detailed in AISI specification [69]. On the other hand, the statistical parameters, M_m = 1.16, F_m = 1.00, V_M = 0.05 and V_F = 0.03 have been adopted for hot-rolled steel, this is consistent with previous studies [70,72,73]. Further, in the estimation of reliability index, correlation factor $C_p = (1+1/n)m/(m-2)$ has also been taken into account for the effect of number of data, where n is the number of data and m is the degree of freedom. A load combination of 1.2DL + 1.6LL, as specified in AISI specification [69], has been adopted to calculate the reliability index for all the design equations. A lower bound value of 2.5 for the reliability index (β) has been considered and the design equation is considered to be reliable if the estimated reliability index is greater than or equal to 2.5.

5.5 Comparison of FE column capacities and current design predictions

The ultimate load (P_{FE}) generated from the FE models of single perforated cold-formed and hot-rolled steel stub module columns subjected to uniform compressive concentric load, generally failed by local buckling and material yielding failure, have been compared with the predicted design strengths (P_{nl-EWM}, P_{nl-DSM}, P_{MP-EC3}, P_{MP-BS}, P_{ARS}, P_{STT}, P_{DS} and P_{SD}) calculated by using the equations set out in AISI S100-16 [39] and those proposed by researchers [9,24,25,40,41]. It may be worth mentioning that the design formulae of AISI S100-16 [39], Miller and Peköz [40], and Abdel-Rahman and Sivakumaran [41] are based on effective area method, whereas the design equation presented by DSM in AISI S100-16 [39], Shanmugam et al. [9], Dhanalakshmi and Shanmugam [25], and Shanmugam and Dhanalakshmi [24] are based on total area method. A total of 258 FE generated module column capacities has been utilised. Detailed comparison of design predictions with FE column capacities for cold-formed and hot-rolled steel are presented in Table 12 and 13, respectively. The mean values (P_m) of the ratio of FE ultimate column capacities to the design predictions, P_{FE}/P_{nl-EWM}, P_{FE}/P_{nl-DSM}, P_{FE}/P_{MP-EC3}, P_{FE}/P_{MP-BS}, P_{FE}/P_{ARS}, P_{FE}/P_{STT}, P_{FE}/P_{DS} and P_{FE}/P_{SD} are 1.04, 1.68, 1.11, 1.11, 1.04, 1.01, 1.69 and 1.03, with corresponding coefficient of variations (COVs) are 0.10, 0.10, 0.05, 0.05, 0.04, 0.09, 0.10 and 0.06 for cold-formed steel module columns. On the other hand, for hot-rolled steel, the mean value of the ratio of FE to the design strengths, P_{FE}/P_{nl-EWM}, P_{FE}/P_{nl-DSM}, P_{FE}/P_{MP-EC3}, P_{FE}/P_{MP-BS}, P_{FE}/P_{ARS}, P_{FE}/P_{STT}, P_{FE}/P_{DS} and P_{FE}/P_{SD} are 1.05, 1.61, 1.05, 1.05, 1.00, 0.95, 1.71 and 0.98 and the corresponding COVs are 0.04, 0.18, 0.04, 0.04, 0.07, 0.06, 0.18 and 0.05. It can be observed from the comparison that, for cold-formed steel module columns, the design predictions by EWM in AISI Standard [39], Miller and Peköz [40], Abdel-Rahman and Sivakumaran [41], Shanmugam et al. [9] and Shanmugam and Dhanalakshmi [24] are slightly conservative whereas the design values by DSM in AISI Standard [39] and Dhanalakshmi and Shanmugam [25] are overly conservative. Moreover, in the case of hot-rolled steel stub columns, the design formulae presented in EWM in AISI Standard [39], Miller and Peköz [40] and Abdel-Rahman and Sivakumaran [41] provide slightly conservative prediction; while the prediction values by DSM in AISI Standard [39] and Dhanalakshmi and Shanmugam [25] are overly conservative. However, the design equation proposed by Shanmugam et al. [9] and Shanmugam and Dhanalakshmi [24] are found to be unconservative for design of hot-rolled steel module stub columns. Further, based on the reliability analysis, it has been observed that, most of the design equations provide reliability index values greater than the lower bound value of 2.5 for both cold-formed and hot-rolled steel module stub columns and hence reliable. Design equations which are developed based on the effective width methods are observed to provide accurate predictions (slightly conservative with lower value of COV) as compared to those which are based on the total area method. Hence, the design equations detailed in AISI Standard [39] and those reported by Miller and

Peköz [40], which are based on effective width method are recommended for the design of perforated module stub columns.

6 Conclusions

This paper presented a comprehensive parametric study to investigate the effects of various key geometric parameters, *viz.*, shape, eccentricity (or location), size (or diameter) and height (or depth) of perforation; and cross-sectional thickness on the buckling capacity of (single) perforated module column subjected to compressive axial load using the commercial FE software ABAQUS. Based on the parametric study, the following conclusions are highlighted:

1) Perforation eccentricity has minor influence on the critical buckling capacity of single perforated module stub columns. For Class 1–3 SHS stub columns having d/w = 0.5, a maximum reduction of about 5% in the column capacity has been observed when the perforation is located at mid-height of the column.

2) The perforation shapes under consideration have been found to have marginal impact on the buckling capacity of the module stub columns, although the reduction in capacity is seen to be in the order - square > hexagon > circular perforated columns (having same perforation size) both for cold-formed and hot-rolled steels.

3) Perforation size (width or diameter of perforation) has major influence on the critical buckling capacity of module column. Overall, the critical buckling capacity of perforated stub module column decreases linearly as perforation size ratio (d/w) increases. Additionally, for similar cross-sectional dimensions and perforation size ratio, perforated cold-formed steel module stub columns offer better cross-sectional performance as compared to those of hot-rolled steel columns.

4) The effect of perforation depth/height on the critical buckling capacity of perforated module column is found to be insignificant. For Class 1–3 SHS stub columns having perforation of size, d/w = 0.7, the increase in perforation height up to 2.5 times the perforation width resulted a reduction in column capacity in the range of ±1.0%.

5) Most of the currently available design formulae for perforated compression member are found to provide conservative and reliable predictions for design of single perforated cold-formed and hot-rolled steel module stub columns.

6) Design equations which are developed based on the effective width methods are observed to provide accurate predictions (slightly conservative with lower value of COV) as compared to those which are based on the total area method. Hence, the design equations detailed in AISI Standard [39] and those reported by Miller and Peköz [40], which are based on effective width method are recommended for the design of perforated module stub columns.

CRediT authorship contribution statement

Tekcham Gishan Singh: Methodology, Software, Validation, Investigation, Codal comparisons; Writing - original draft. Tak-Ming Chan: Conceptualization, Methodology, Writing - review & editing, Supervision, Funding acquisition.

Declaration of competing interest

No potential conflict of interest was reported by the authors.

Acknowledgements

The authors sincerely acknowledges the support from the Innovation and Technology Fund - Nano and Advanced Materials Institute (ITF-NAMI) for the project "Hong Kong Modular Integrated Construction (MiC) Innovations" (PolyU/ ZS12) and from the Chinese National Engineering Research Centre for Steel Construction (Hong Kong Branch) at The Hong Kong Polytechnic University.

References

[1] Chen Z., Liu J., Yu Y., Experimental study on interior connections in modular steel buildings, Eng. Struct. 147 (2017) 625–638.

[2] Chen Z., Liu J., Yu Y., Zhou C., Yan R., Experimental study of an innovative modular steel building connection, J. Constr. Steel Res. 139 (2017) 69–82.

[3] Lacey A.W., Chen W., Hao H., Bi K., Review of bolted inter-module connections in modular steel buildings, J. Build. Eng. 23 (2019) 207–219.

[4] Lacey A.W., Chen W., Hao H., Bi K., Tallowin F.J., Shear behaviour of post-tensioned inter-module connection for modular steel buildings, J. Constr. Steel Res. 162 (2019) 105707.

[5] Choi K.-S., Lee H.-C., Kim H.-J., Influence of analytical models on the seismic response of modular structures, J. Korea Inst. Struct. Maint. Insp. 20 (2016) 74–85.

[6] Liu M., Zhu X., Wang P., Tuoya W., Hu S., Tension strength and design method for thread-fixed one-side bolted T-stub, Eng. Struct. 150 (2017) 918–933.

[7] Ritchie D., Rhodes J., Buckling and post-buckling behaviour of plates with holes, Aeronaut. Q. 26 (1975) 281–296.

[8] Larsson P.-L., On buckling of orthotropic compressed plates with circular holes, Compos. Struct. 7(1987) 103–121.

[9] Shanmugam N.E., Thevendran V., Tan Y.H., Design formula for axially compressed perforated plates, Thin-Walled Struct. 34 (1999) 1–20.

[10] Cheng B., Wang J., Li C., Compression behavior of perforated plates in steel tower anchorage zones of cable-stayed bridges, J. Constr. Steel Res. 90 (2013) 72–84.

[11] Saad-Eldeen S., Garbatov Y., Guedes Soares C., Experimental strength assessment of thin steel plates with a central elongated circular opening, J. Constr. Steel Res. 118 (2016) 135–144.

[12] Saad-Eldeen S., Garbatov Y., Guedes Soares C., Experimental failure assessment of high tensile stiffened plates with openings, Eng. Struct. 206 (2020) 110121.

[13] Saad-Eldeen S., Garbatov Y., Guedes Soares C., Buckling collapse tests of deteriorated steel plates with multiple circular openings, Ocean Eng. 172 (2019) 523–530.

[14] Yu W.-W., Davis C.S., Cold-formed steel members with perforated elements, J. Struct. Div. 99 (1973) 2061–2077.

[15] Sonu J.K., Singh K.D., Shear behaviour of single perforated lean duplex stainless steel (LDSS) rectangular hollow beams, Thin-Walled Struct. 119 (2017) 851–867.

[16] Lagaros N.D., Psarras L.D., Papadrakakis M., Panagiotou G., Optimum design of steel structures with web openings, Eng. Struct. 30 (2008) 2528–2537.

[17] Zaher O.F., Yossef N.M., El-Boghdadi M.H., Dabaon M.A., Structural behaviour of arched steel beams with cellular openings, J. Constr. Steel Res. 148 (2018) 756–767.

[18] Zhou F., Young B., Web crippling of aluminium tubes with perforated webs, Eng. Struct. 32 (2010) 1397–1410.

[19] Feng R., Chen Z., Shen C., Roy K., Chen B., Lim J.B.P., Flexural capacity of perforated aluminium CHS tubes–an experimental study, Structures, Elsevier, 2020, pp. 463–480.

[20] Feng R., Sun W., Shen C., Zhu J., Experimental investigation of aluminum square and rectangular beams with circular perforations, Eng. Struct. 151 (2017) 613–632.

[21] N.S. Marshall, G.N. Nurick, The effect of induced imperfections on the formation of the first lobe of symmetric progressive buckling of thin-walled square tubes, WIT Trans. Built Environ. 35 (1970) 0–14.

[22] Jullien J.F., Limam A., Effects of openings of the buckling of cylindrical shells subjected to axial compression, Thin-Walled Struct. 31 (1998) 187–202.

[23] Pu Y., Godley M.H.R., Beale R.G., Lau H.H., Prediction of ultimate capacity of perforated lipped channels, J. Struct. Eng. 125 (1999) 510–514.

[24] Shanmugam N.E., Dhanalakshmi M., Design for openings in cold-formed steel channel stub columns, Thin-Walled Struct. 39 (2001) 961–981.

[25] Dhanalakshmi M., Shanmugam N.E., Design for openings in equal-angle cold-formed steel stub columns, Thin-Walled Struct. 39 (2001) 167–187.

[26] Yao Z., Rasmussen K.J.R., Inelastic local buckling behaviour of perforated plates and sections under compression, Thin-Walled Struct. 61 (2012) 49–70.

[27] Umbarkar K.R., Patton L.M., Singh K.D., Effect of single circular perforation in lean duplex stainless steel (LDSS) hollow circular stub columns under pure axial compression, Thin-Walled Struct. 68 (2013) 18–25.

[28] Feng R., Young B., Experimental investigation of aluminum alloy stub columns with circular openings, J. Struct. Eng. 141 (2015) 4015031.

[29] Singh T.G., Singh K.D., Experimental investigation on performance of perforated cold–formed steel tubular stub columns, Thin-Walled Struct. 131 (2018) 107–121.

[30] Feng R., Zhu W., Wan H., Chen A., Chen Y., Tests of perforated aluminium alloy SHSs and RHSs under axial compression, Thin-Walled Struct. 130 (2018) 194–212.

[31] Devi S.V., Singh T.G., Singh K.D., Cold-formed steel square hollow members with circular perforations subjected to torsion, J. Constr. Steel Res. 162 (2019) 105730.

[32] Devi S.V., Singh K.D., Finite element study of lean duplex stainless steel semi-elliptical hollow section members with circular perforation subjected to torsion, Thin-Walled Struct. 146 (2020) 106464.

[33] Moen C.D., Schafer B.W., Experiments on cold-formed steel columns with holes, Thin-Walled Struct. 46 (10) (2008) 1164–1182.

[34] Feng R., Liu J., Numerical investigation and design of perforated aluminium alloy SHS and RHS columns, Eng. Struct. 199 (2019) 109591.

[35] Gardner L., Yun X., Description of stress-strain curves for cold-formed steels, Constr. Build. Mater. 189 (2018) 527–538.

[36] Yun X., Gardner L., Stress-strain curves for hot-rolled steels, J. Constr. Steel Res. 133 (2017) 36–46.

[37] Nseir J., Development of a New Design Method for the Cross-Section Capacity of Steel Hollow Sections (PhD Thesis) Université de Liège, Liège, Belgique, 2015.

[38] Liew A., Design of structural steel elements with the Continuous Strength Method (PhD Thesis) Imperial College London, 2014.

[39] AISI S100-16, North American Specification for the Design of Cold-Formed Steel Structural Members, Am. Iron Steel Inst. (AISI), Washington, DC, 2016.

[40] Miller T.H., Peköz T., Unstiffened strip approach for perforated wall studs, J. Struct. Eng. 120 (1994) 410–421.

[41] Abdel-Rahman N., Sivakumaran K.S., Effective design width for perforated cold-formed steel compression members, Can. J. Civ. Eng. 25 (1998) 319–330.

[42] Tata Steel, Tata Steel Production Manual for YSt 310 Rectangular, Square and Circular Steel Hollow Section, Tata Steel Limited, Kolkata, 2013.

[43] IS 4923, Hollow Steel Sections for Structural Use – Specification, Indian Stand. Bur. Indian Stand., New Delhi, 1997.

[44] Dawson R.G., Walker A.C., Post-buckling of geometrically imperfect plates, J. Struct. Div. 98 (1972) 75–94.

[45] ABAQUS/Standard, Version 6.13-1, K. a. S. Hibbit, USA, 2013.

[46] Singh T.G., Singh K.D., Structural performance of YSt–310 cold–formed tubular steel stub columns, Thin-Walled Struct. 121 (2017) 25–40.

[47] Singh T.G., Structural Performance of YSt-310 Cold-Formed Steel Tubular Columns PhD Thesis Indian Institute of Technology Guwahati (India), 2019.

[48] Theofanous M., Gardner L., Testing and numerical modelling of lean duplex stainless steel hollow section columns, Eng. Struct. 31 (2009) 3047–3058.

[49] Fang H., Chan T.-M., Young B., Behavior of octagonal high-strength steel tubular stub columns, J. Struct. Eng. 145 (2019) 4019150.

[50] Theofanous M., Gardner L., Experimental and numerical studies of lean duplex stainless steel beams, J. Constr. Steel Res. 66 (2010) 816–825.

[51] Sachidananda K., Singh K.D., Numerical study of fixed ended lean duplex stainless steel (LDSS) flat oval hollow stub column under pure axial compression, Thin-Walled Struct. 96 (2015) 105–119.

[52] Yu C., Schafer B.W., Effect of longitudinal stress gradients on elastic buckling of thin plates, J. Eng. Mech. 133 (4) (2007) 452–463.

[53] Chan T.M., Gardner L., Compressive resistance of hot-rolled elliptical hollow sections, Eng. Struct. 30 (2008) 522–532.

[54] Gardner L., Nethercot D.A., Numerical modeling of stainless steel structural components—a consistent approach, J. Struct. Eng. 130 (2004) 1586–1601.

[55] EN 10025-2, Hot Rolled Products of Structural Steels - Part 2: Technical Delivery Conditions for NonAlloy Structural Steels, CEN, Brussels, 2004.

[56] Mirambell E., Real E., On the calculation of deflections in structural stainless steel beams: an experimental and numerical investigation, J. Constr. Steel Res. 54 (2000) 109–133.

[57] Somodi B., Kövesdi B., Residual stress measurements on cold-formed HSS hollow section columns, J. Constr. Steel Res. 128 (2017) 706–720.

[58] Huang Y., Young B., Material properties of cold-formed lean duplex stainless steel sections, Thin-Walled Struct. 54 (2012) 72–81.

[59] Young B., Lui W.-M., Behavior of cold-formed high strength stainless steel sections, J. Struct. Eng. 131 (2005) 1738–1745.

[60] Ma J.-L., Chan T.-M., Young B., Experimental investigation on stub-column behavior of cold-formed high-strength steel tubular sections, J. Struct. Eng. 142 (2016) 4015174.

[61] Ellobody E., Young B., Structural performance of cold-formed high strength stainless steel columns, J. Constr. Steel Res. 61 (2005) 1631–1649.

[62] Huang Y., Young B., Structural performance of cold-formed lean duplex stainless steel columns, Thin-Walled Struct. 83 (2014) 59–69.

[63] Ziemian R.D., Guide to Stability Design Criteria for Metal Structures, Sixth ed., John Wiley & Sons, 2010.

[64] EN 1993-1-1, Eurocode 3: Design of Steel Structures–Part 1–1: General Rules and Rules for Buildings, Eur. Stand. Eur. Comm. Stand. (CEN), Brussels, 2005.

[65] Moen C.D., Schafer B.W., Direct strength method for design of cold-formed steel columns with holes, J. Struct. Eng. 137 (2011) 559–570.

[66] EC3-1-5, Eurocode 3: Design of Steel Structures–Part 1–5: Plated Structural Elements, Eur. Comm. Stand. (CEN), Brussels,2006.

[67] AS/NZS 4600, Cold-Formed Steel Structures, Australian/New Zealand Standards, New Zealand, 2005.

[68] BS 5950-5, Structural Use of Steelwork in building – Part 5: Code of Practice for Design of Cold Formed Thin Gauge Sections, Br. Stand. Inst., 1998.

[69] AISI S100-16C, Commentary on North American Specification for the Design of Cold-Formed Steel Structural Members, Am. Iron Steel Inst. (AISI), Washington, DC, 2016.

[70] Cai Y., Quach W.-M., Chen M.-T., Young B., Behavior and design of cold-formed and hot-finished steel elliptical tubular stub columns, J. Constr. Steel Res. 156 (2019) 252–265.

[71] AISC 360, Specification for Structural Steel Buildings, ANSI/AISC 360-10, American Institution of Steel Construction, Chicago, 2010.

[72] Yun X., Gardner L., Boissonnade N., The continuous strength method for the design of hot-rolled steel cross-sections, Eng. Struct. 157 (2018) 179–191.

[73] Byfield M.P., Nethercot D.A., Material and geometric properties of structural steel for use in design, Struct. Eng. 75 (1997).

Notations

A_e	Effective area calculated at stress F_n
A_0	Total surface area of perforations
A_g	Gross cross-sectional area
A_{net}	Cross-sectional area perforated column at the location of perforation
A_s	Total surface area of the member;
b	Effective width
B	Width of cross-section
b_{DW}	Effective design width
CF	Cold-formed steel material
COV	Coefficient of variance
C_p	Correction factor
d	Diameter of perforation/hole/cut-out/opening
D	Depth of cross-section
d/w	Perforation size ratio
DL	Dead load
DSM	Direct Strength Method
e	Distance between the perforation centre to the unloaded end of stub column
E	Young’s modulus of elasticity
e/L	Eccentricity of perforation
$E_{0.2}$	Tangent modulus at the 0.2% proof stress
EH	Equal perforation height
EWM	Effective width method
f	Stress
f_{cr}	Critical elastic buckling stress for unperforated plate elements
f_{crl}	Minimum elastic buckling stress
f_{cr-p}	Critical elastic buckling stress for perforated plate elements
FE	Finite element
F_m	Mean value of fabrication factor
$F_{\max}$	Maximum design stress
F_n	Global column stress
f_u	Ultimate strength
f_y	0.2% proof stress
H	Height/depth of perforation
HR	Hot-rolled steel material
k	Plate buckling coefficient
K	Effective length factor
k_h	Plate buckling coefficient for perforated element
k_1, k_2 *and* k_3	Sets of coefficients
L	Overall length of stub column
LDSS	Lean duplex stainless steel
LL	Live load
LVDT	Linear variable displacement transducers
m	Strain hardening component for the curves after yield stress or plate slenderness ratio or degree of freedom
M_m	Mean value of material factor
MSC	Modular steel construction
n	Strain hardening exponent or number of data
P	Axial compressive load

P_0	Critical buckling load of unperforated stub column
$P_{1.0}$	Critical buckling capacity with perforation height to width ratio is 1.0
P_{ARS}	Column capacity by Abdel-Rahman and Sivakumaran [41]
P_{crl}	Critical elastic buckling load
P_{DS}	Un-factored design strength based on Dhanalakshmi and Shanmugam [25]
P_{FE}	Numerical ultimate load
P_m	Mean value
P_{MP-EC3}	Column capacity proposed by Miller and Peköz [40] simplified formula detailed in EC3-1-5 [66]
P_{MP-BS}	Column capacity proposed by Miller and Peköz [40] simplified formula detailed in BS 5950–5 [68]
P_{nd}	Nominal axial strength of column undergoing distortional buckling
P_{ne}	Nominal strength considering yielding and global buckling
P_{nl}	Nominal axial strength of column undergoing local buckling
$P_{nl\text{-}DSM}$	Nominal axial strength for local buckling based on DSM
$P_{nl\text{-}EWM}$	Nominal axial strength for local buckling based on EWM
P_{SD}	Un-factored design strength based on Shanmugam and Dhanalakshmi [24]
PSHS	Perforated square hollow section
P_{sq}	Squash load
P_{STT}	Un-factored design strength based on Shanmugam et al. [9]
P_{Test}	Experimental ultimate capacity
P_u	Critical buckling load of perforated stub column
P_y	Yield load
P_{ynet}	Member yield strength on net cross-section
RHS	Rectangular hollow sections
r_i	Inner corner radius
SHS	Square hollow sections
t	Section thickness
USHS	Unperforated square hollow section
V_F	Coefficient of variation of fabrication factor
V_M	Coefficient of variation of material factor
V_p	Coefficient of variation
w	Flat element width
w_h	Equivalent unstiffened plate element width
β	Reliability index
δ	Deformation or end-shortening
δ_u	Deformation corresponding to ultimate load
ε	Strain or material factor
$\varepsilon_{0.2}$	Total strain at the 0.2% proof stress
ε_f	Percentage elongation at fracture
$\varepsilon_{\ln}^{pl}$	Logarithmic plastic strain
ε_{nom}	Engineering strain
ε_{sh}	Strain hardening strain
ε_u	Strain corresponding to ultimate stress
ε_y	Strain corresponding to yield stress
λ	Slenderness factor
λ_l	Slenderness factor for local buckling of column

$\overline{\lambda}_p$	Cross-sectional slenderness
υ	Poisson's ratio
ω_0	Local geometric imperfection amplitude proposed by Singh and Singh [29]
ϕ	Resistance factor
σ_{nom}	Engineering stress
σ_{true}	True stress

Table 1. Geometric dimensions of perforated stub columns [29].

Cross-sections[a]	B (mm)	D (mm)	t (mm)	L (mm)	r_i (mm)	w (mm)	d (mm)	d/w
50 × 50 × 2.9*d*/*w*0.5–1	49.56	49.82	2.89	200.20	2.9	37.98	19.2	0.51
50 × 50 × 2.9*d*/*w*0.7–1	49.82	49.88	2.90	199.96	2.9	38.22	26.9	0.70
50 × 50 × 2.9*d*/*w*0.9–1	49.62	49.82	2.91	200.36	2.9	38.00	34.6	0.91
60 × 60 × 2.6*d*/*w*0.1–1	60.00	60.10	2.61	200.00	2.6	48.98	5.00	0.10
60 × 60 × 2.6*d*/*w*0.3–1	60.00	60.10	2.61	200.22	2.6	48.98	14.9	0.30
60 × 60 × 2.6*d*/*w*0.3–2	59.90	60.12	2.61	200.10	2.6	48.88	14.9	0.30
60 × 60 × 2.6*d*/*w*0.5–1	60.04	60.08	2.62	199.96	2.6	49.00	24.8	0.51
60 × 60 × 2.6*d*/*w*0.5–2	60.00	60.10	2.62	200.00	2.6	48.96	24.8	0.51
60 × 60 × 2.6*d*/*w*0.7–1	60.00	60.18	2.60	199.94	2.6	49.00	34.7	0.71
60 × 60 × 2.6*d*/*w*0.7–2	59.92	60.12	2.61	200.08	2.6	48.90	34.7	0.71
60 × 60 × 2.6*d*/*w*0.9–1	59.94	60.00	2.59	200.00	2.6	48.96	44.6	0.91
60 × 60 × 2.6*d*/*w*0.9–2	59.94	60.00	2.62	200.00	2.6	48.90	44.6	0.91
60 × 40 × 2.9*d*/*w*0.1–1	60.13	40.13	2.91	160.23	2.9	48.51	4.80	0.10
60 × 40 × 2.9*d*/*w*0.3–1	60.18	40.28	2.91	160.06	2.9	48.56	14.5	0.30
60 × 40 × 2.9*d*/*w*0.5–1	60.14	40.16	2.89	160.10	2.9	48.56	24.2	0.50
60 × 40 × 2.9*d*/*w*0.7–1	60.11	40.30	2.90	160.10	2.9	48.51	33.9	0.70
60 × 40 × 2.9*d*/*w*0.7–2	60.16	40.21	2.90	160.22	2.9	48.56	33.9	0.70
60 × 40 × 2.9*d*/*w*0.9–1	60.11	40.22	2.87	159.32	2.9	48.57	43.6	0.90
60 × 40 × 2.9*d*/*w*0.9–2	60.14	40.23	2.88	160.30	2.9	48.56	43.6	0.90

[a] Cross-sectional nomenclatures are based on [29].

Table 2. Flat coupon material properties for YSt-310 cold-formed steels [46].

Cross-sections[a]	E (N/mm^2)	f_y (N/mm^2)	f_u (N/mm^2)	ε_f (%)	n
50 × 50 × 2.9	190,024	370	446.48	22.56	4.2
60 × 40 × 2.9	201,845	408	439.35	18.33	5.7
60 × 60 × 2.6	204,082	431	483.24	17.76	4.1

[a] Cross-sectional nomenclatures are based on [46].

Table 3. Corner coupon material properties for YSt-310 cold-formed steels [46].

Cross-sections[a]	E (N/mm^2)	f_y (N/mm^2)	f_u (N/mm^2)	ε_f (%)	n
50 × 50 × 2.9	176,191	506	571.53	7.69	2.7
60 × 40 × 2.9	187,050	502	569.90	8.80	3.5
60 × 60 × 2.6	192,308	556	689.31	11.53	2.5

[a] Cross-sectional nomenclatures are based on [46].

Table 4. Comparison of test results with FE ultimate column capacities and corresponding displacements.

Cross-sections[a]	P_{Test} (kN)	P_{Test}/P_{FE}		
		ω_0	$t/10$	$t/100$
50 × 50 × 2.9*d*/*w*0.5–1	207.99	1.00	0.98	1.00
50 × 50 × 2.9*d*/*w*0.7–1	187.16	1.00	1.02	1.01
50 × 50 × 2.9*d*/*w*0.9–1	159.44	0.99	1.02	1.00
60 × 60 × 2.6*d*/*w*0.1–1	295.65	1.01	1.07	1.01
60 × 60 × 2.6*d*/*w*0.3–1	271.65	1.00	1.03	1.00
60 × 60 × 2.6*d*/*w*0.3–2	274.38	1.01	1.04	1.01
60 × 60 × 2.6*d*/*w*0.5–1	254.21	1.05	1.03	1.04
60 × 60 × 2.6*d*/*w*0.7–1	216.72	1.02	1.05	1.02
60 × 60 × 2.6*d*/*w*0.7–2	214.89	1.01	1.04	1.01
60 × 60 × 2.6*d*/*w*0.9–1	181.20	1.00	0.95	1.00
60 × 60 × 2.6*d*/*w*0.9–2	183.95	1.00	0.95	0.99
60 × 40 × 2.9*d*/*w*0.1–1	256.56	1.02	1.06	1.03
60 × 40 × 2.9*d*/*w*0.3–1	229.63	1.00	1.02	1.00
60 × 40 × 2.9*d*/*w*0.5–1	205.75	1.02	1.02	1.03
60 × 40 × 2.9*d*/*w*0.7–1	174.43	1.01	1.02	1.01
60 × 40 × 2.9*d*/*w*0.7–2	176.03	1.02	1.03	1.02
60 × 40 × 2.9*d*/*w*0.9–1	143.09	0.99	0.98	0.99
60 × 40 × 2.9*d*/*w*0.9–2	145.39	1.01	1.00	1.01
Mean		1.01	1.02	1.01
COV		0.01	0.03	0.01

[a] Cross-sectional nomenclatures are based on [29].

Table 5. Flat coupon material properties for S355 cold-formed steel detailed in Nseir [37].

Cross-sections[a]	E (N/mm^2)	f_y (N/mm^2)	f_u (N/mm^2)	ε_u	n	m
RHS-S355CF-200 × 100 × 4.0	216,630	494.60	611.00	11.90		
RHS-S355CF-220 × 120 × 6.0	206,597	454.70	563.60	15.50		
RHS-S355CF-200 × 200 × 5.0	214,848	480.20	585.00	14.50	7.6	3.8
RHS-S355CF-200 × 200 × 6.0	217,363	500.50	596.00	13.80		
Mean	213,860	482.50	588.90	13.93		

[a] Cross-sectional nomenclatures are based on [37].

Table 6. Corner coupon material properties for S355 cold-formed steel detailed in Nseir [37].

Cross-sections[a]	E (N/mm^2)	f_y (N/mm^2)	f_u (N/mm^2)	ε_u	n	m
RHS-S355CF-200 × 100 × 4.0	213,000	580.00	601.15	1.20		
RHS-S355CF-220 × 120 × 6.0	207,000	599.27	644.00	1.25		
RHS-S355CF-200 × 200 × 5.0	209,500	531.00	573.35	1.24	7.0	4.2
RHS-S355CF-200 × 200 × 6.0	210,500	578.00	617.80	1.10		
Mean	210,000	572.07	609.08	1.20		

[a] Cross-sectional nomenclatures are based on [37].

Table 7. Flat coupon material properties for S355 hot-rolled steel reported by Liew [38].

Identification[a]	E (N/mm^2)	f_y (N/mm^2)	f_u (N/mm^2)	ε_u
41T	203600	436.00	534.00	16.63
42T	198200	423.00	524.00	17.13
43T	207700	419.00	521.00	17.48
44T	208300	423.00	523.00	17.60
51T	197300	396.00	503.00	18.45
51T	207700	401.00	506.00	18.53
51T	203000	400.00	509.00	18.55
51T	206100	395.00	506.00	18.90
Mean	203988	411.63	515.75	17.91

[a] Cross-sectional nomenclature are based on [38].

Table 8. Geometric dimensions of cold-formed steel stub column detailed in Nsier [37].

Cross-sections[a]	B (mm)	D (mm)	t (mm)	L (mm)
RHS-S355CF-200 × 100 × 4.0	200.50	100.28	3.69	600.0
RHS-S355CF-220 × 120 × 6.0	220.60	120.02	5.85	600.0
RHS-S355CF-200 × 200 × 5.0	200.00	201.50	4.72	600.0
RHS-S355CF-200 × 200 × 6.0	200.00	199.70	5.90	600.0

[a] Cross-sectional nomenclatures are based on [37].

Table 9. Geometric dimensions of hot-rolled steel stub column detailed in Liew [38].

Cross-sections ID[a]	B^b	D^b	t^b	L
	(mm)	(mm)	(mm)	(mm)
1ST4	119.71	80.13	3.87	368.0
2ST4	119.69	80.07	3.88	369.0
3ST4	119.72	80.24	3.90	366.0
4ST4	119.61	80.12	3.91	369.0
1ST5	119.65	80.23	4.78	368.0
2ST5	119.76	80.23	4.76	366.0
3ST5	119.71	80.30	4.76	368.0
4ST5	119.75	80.26	4.75	368.0

[a] Cross-sectional nomenclature are based on [38].

[b]Average geometric dimensions are reported.

Table 10. Comparison of test and FE ultimate loads for varying imperfection amplitudes, for validation of cold-formed steel material properties [37].

Cross-sections[a]	P_{Test} (kN)	P_{Test}/P_{FE}		
		ω_0	$t/10$	$t/100$
RHS-S355CF-200 × 100 × 4.0	761.00	0.96	0.97	0.96
RHS-S355CF-220 × 120 × 6.0	1648.00	0.96	1.05	0.97
RHS-S355CF-200 × 200 × 5.0	1296.00	0.93	1.00	0.92
RHS-S355CF-200 × 200 × 6.0	1957.00	0.91	0.99	0.94
Mean		0.94	1.00	0.95
COV		0.03	0.03	0.02

[a] Cross-sectional nomenclature are based on [37].

Table 11. Comparison of test and FE ultimate loads for varying imperfection amplitudes, for validation of hot-rolled steel material properties [38].

Cross-sections[a]	P_{Test} (kN)	P_{Test} / P_{FE}		
		ω_0	t /10	t /100
1ST4	677.92	1.02	1.04	1.02
2ST4	665.90	1.04	1.05	1.04
3ST4	668.37	1.04	1.06	1.04
4ST4	663.15	1.02	1.04	1.03
1ST5	736.14	0.99	1.01	0.99
2ST5	725.19	0.97	0.99	0.97
3ST5	745.54	0.99	1.01	1.00
4ST5	740.99	1.01	1.03	1.01
Mean		1.01	1.03	1.01
COV		0.03	0.02	0.02

[a] Cross-sectional nomenclature are based on [38].

Table 12. Comparison of FE column capacities against the design prediction for cold-formed steel module columns.

	P_{FE}							
	$P_{nl\text{-}EWM}$	$P_{nl\text{-}DSM}$	$P_{MP\text{-}EC3}$	$P_{MP\text{-}BS}$	P_{ARS}	P_{STT}	P_{DS}	P_{SD}
No. of Observation (n)	130	130	130	130	130	130	130	130
Mean (P_m)	1.04	1.68	1.11	1.11	1.04	1.01	1.69	1.03
COV (V_p)	0.10	0.10	0.05	0.05	0.04	0.09	0.10	0.06
Reliability index (β)	2.79	4.67	3.24	3.24	3.00	2.72	4.69	2.91

Table 13. Comparison of FE column capacities against the design prediction for hot-rolled steel module columns.

	P_{FE}							
	$P_{nl\text{-}EWM}$	$P_{nl\text{-}DSM}$	$P_{MP\text{-}EC3}$	$P_{MP\text{-}BS}$	P_{ARS}	P_{STT}	P_{DS}	P_{SD}
No. of Observation (n)	128	128	128	128	128	128	128	128
Mean (P_m)	1.05	1.61	1.05	1.05	1.00	0.95	1.71	0.98
COV (V_p)	0.04	0.18	0.04	0.04	0.07	0.06	0.18	0.05
Reliability index (β)	3.76	4.41	3.76	3.76	3.38	3.18	4.08	3.38

(a)

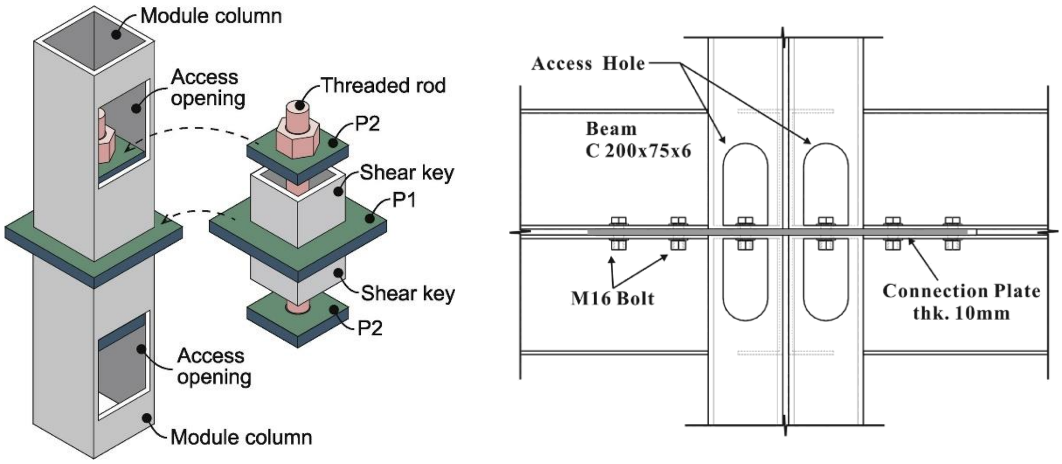

(b)

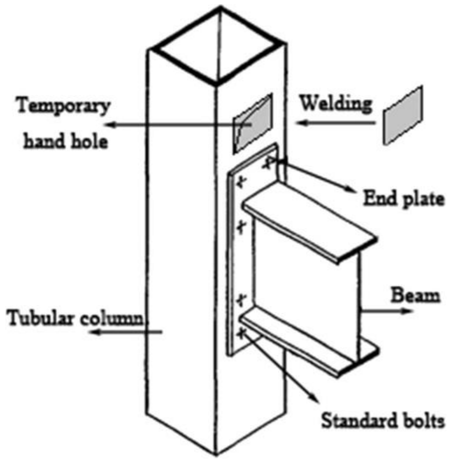

Fig. 1. Access openings are provided for various engineering applications: a) inter-module connections [4,5] and b) beam-column connection [6].

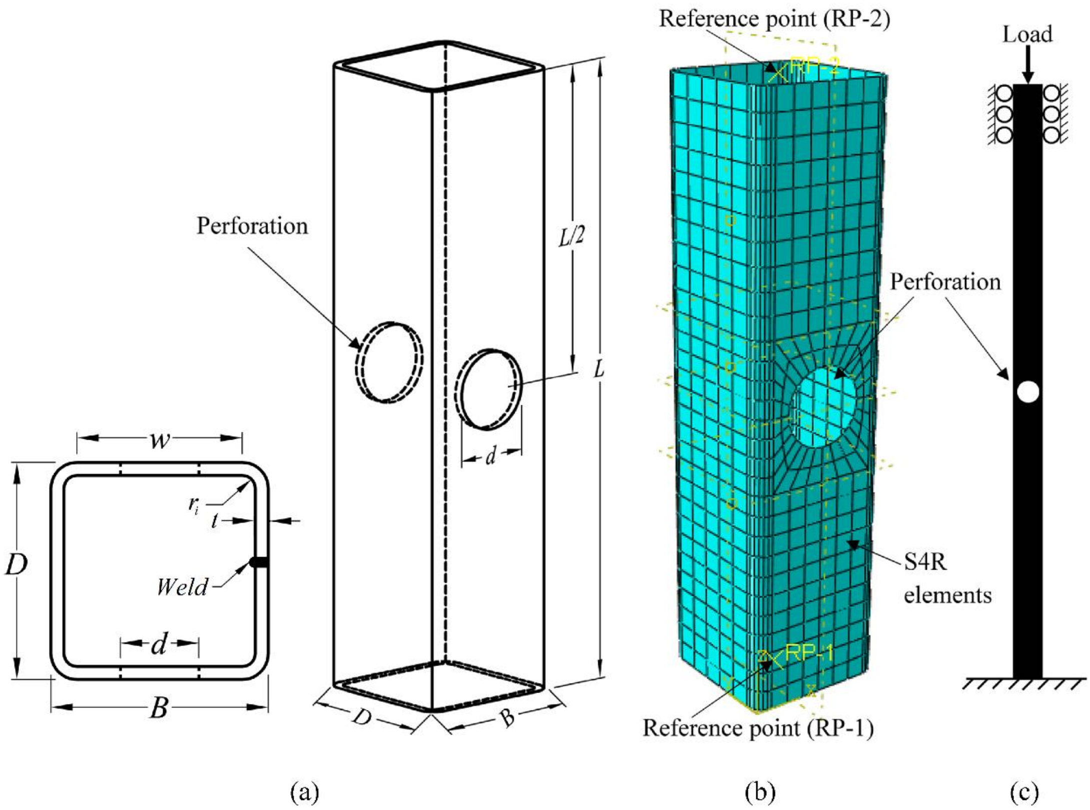

Fig. 2. (a) Definition of symbols in plan and three-dimensional views, (b) typical FE model and (c) boundary conditions for perforated cold-formed steel tubular stub column.

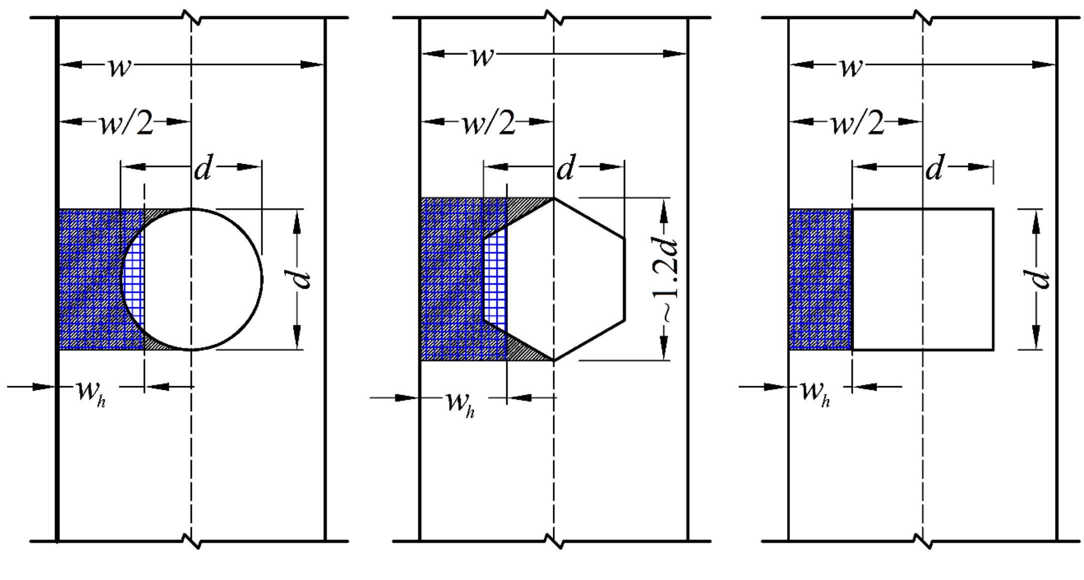

Fig. 3. Equivalent unstiffened plate element width, w_h for (a) circular, (b) hexagonal and (c) square perforations at the location of perforation.

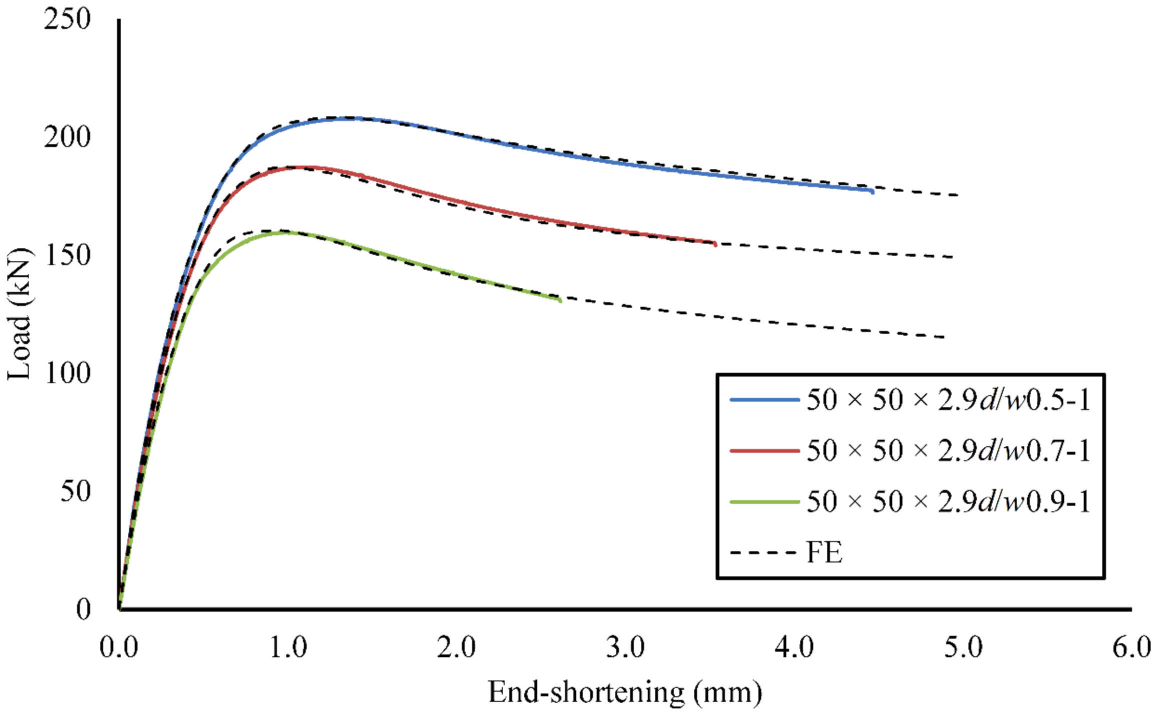

Fig. 4. Test (reported by Singh and Singh [29]) and numerical load versus end-shortening curves for perforated 50 × 50 × 2.9.

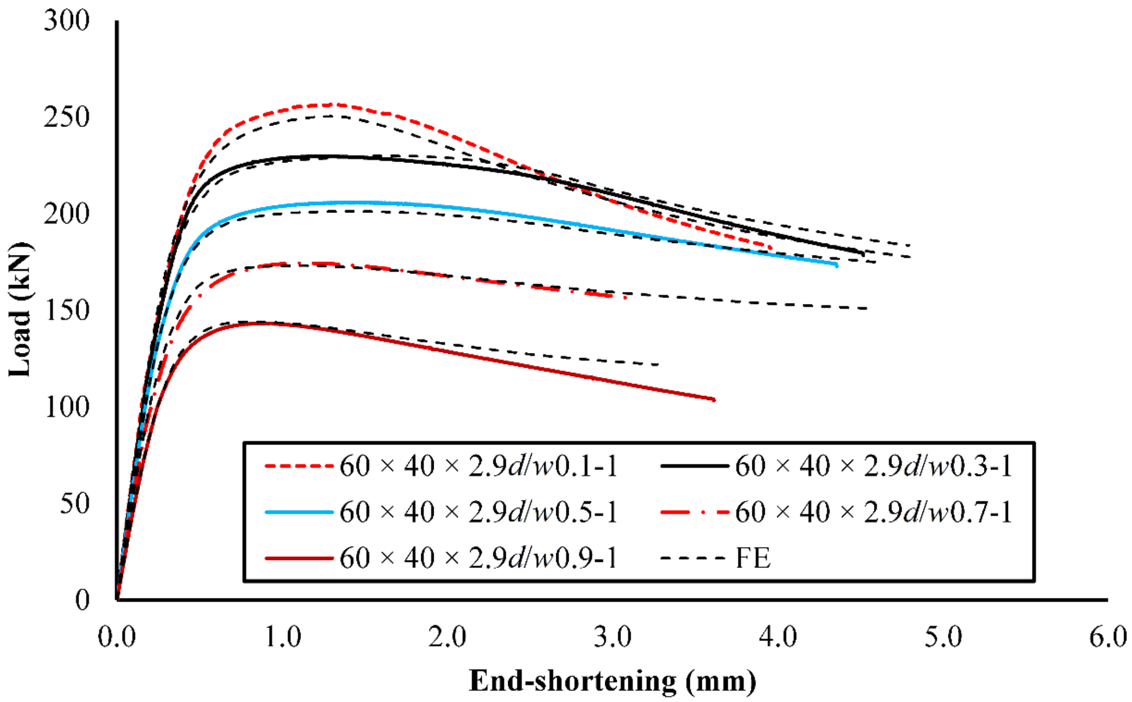

Fig. 5. Experimental (reported by Singh and Singh [29]) and numerical load versus end-shortening curves for 60 × 40 × 2.9.

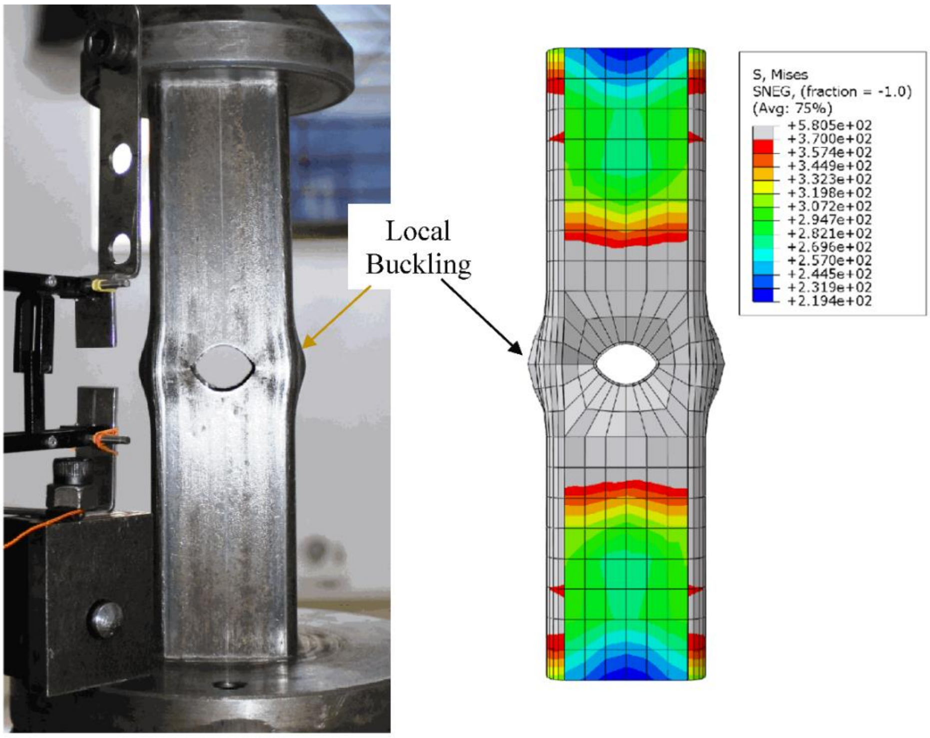

Fig. 6. Comparison of experimental (reported by Singh and Singh [29])and numerical failure modes for SHS 50 × 50 × 2.9*d*/w0.5–1 stub column.

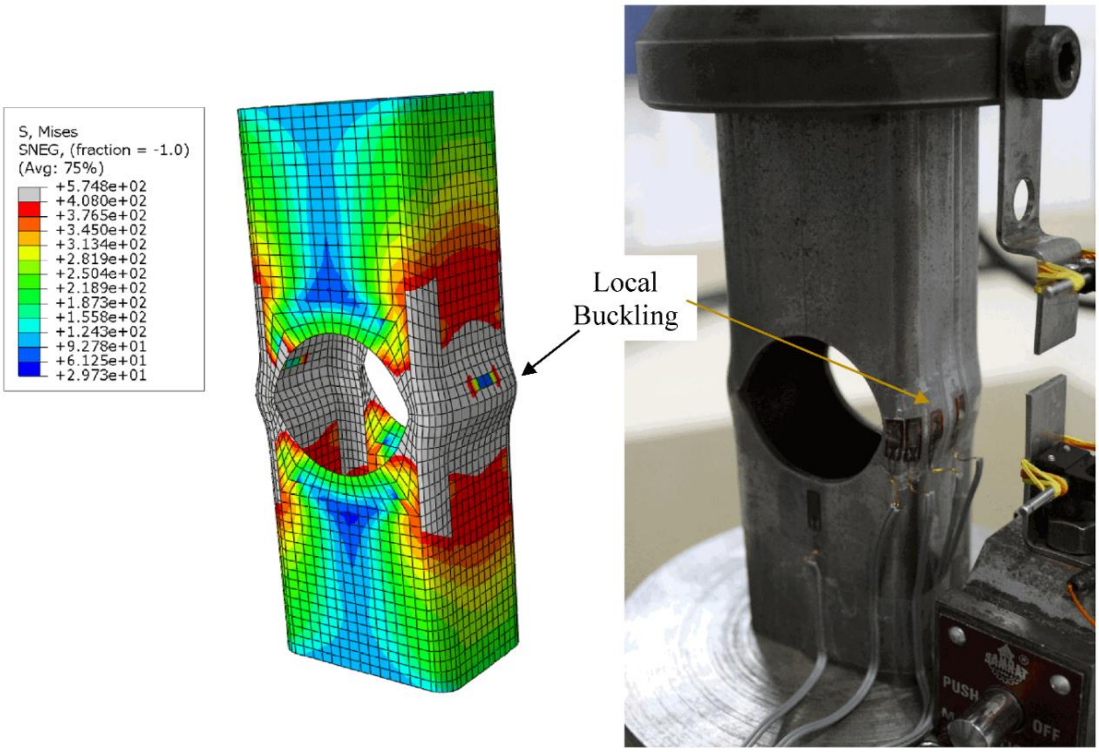

Fig. 7. Deformed mode shapes of FE and experimental - 60 × 40 × 2.9*d*/*w*0.9–2 stub columns (reported by Singh and Singh [29]).

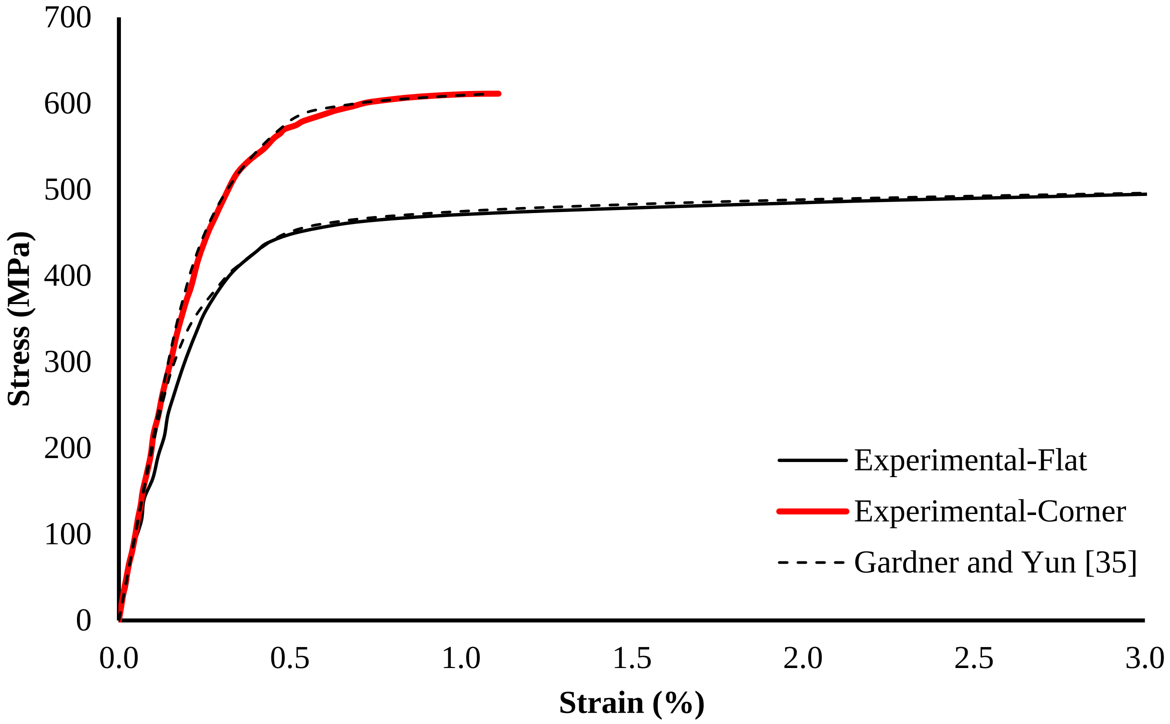

Fig. 8. Comparison of test and material model generated using Gardner and Yun [35] for cold-formed steel S355 reported by Nseir [37].

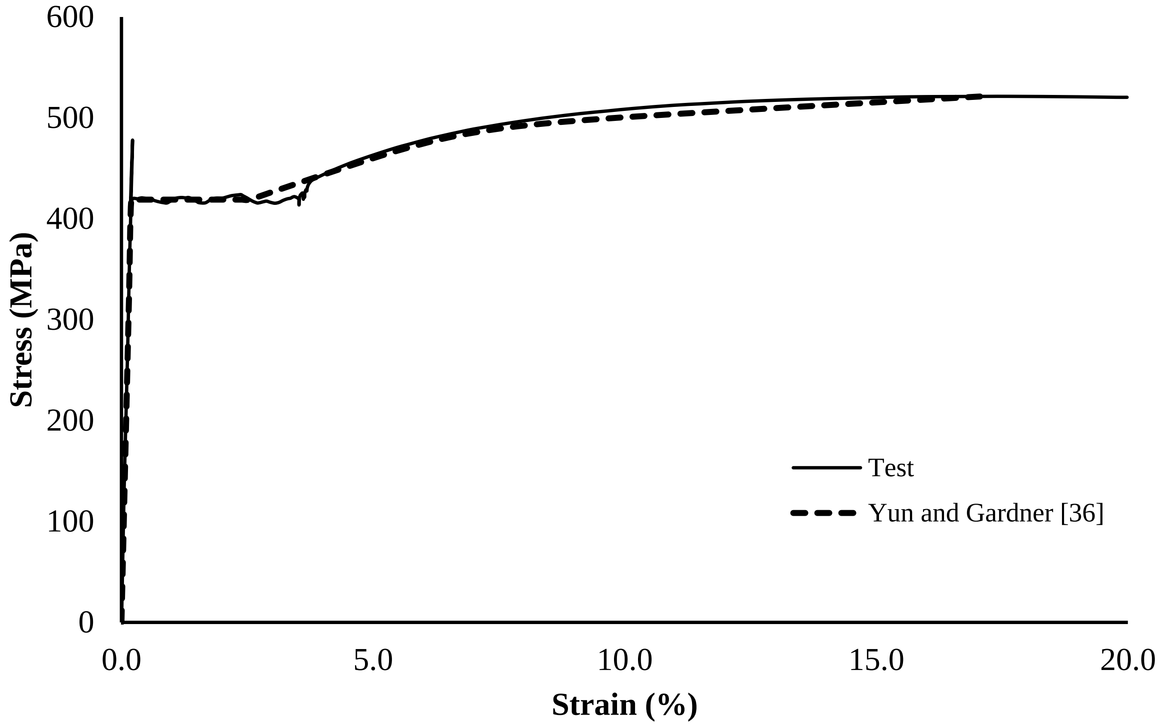

Fig. 9. Comparison of test and material model generated using Yun and Gardner [36] for hot-rolled steel S355 reported by Liew [38].

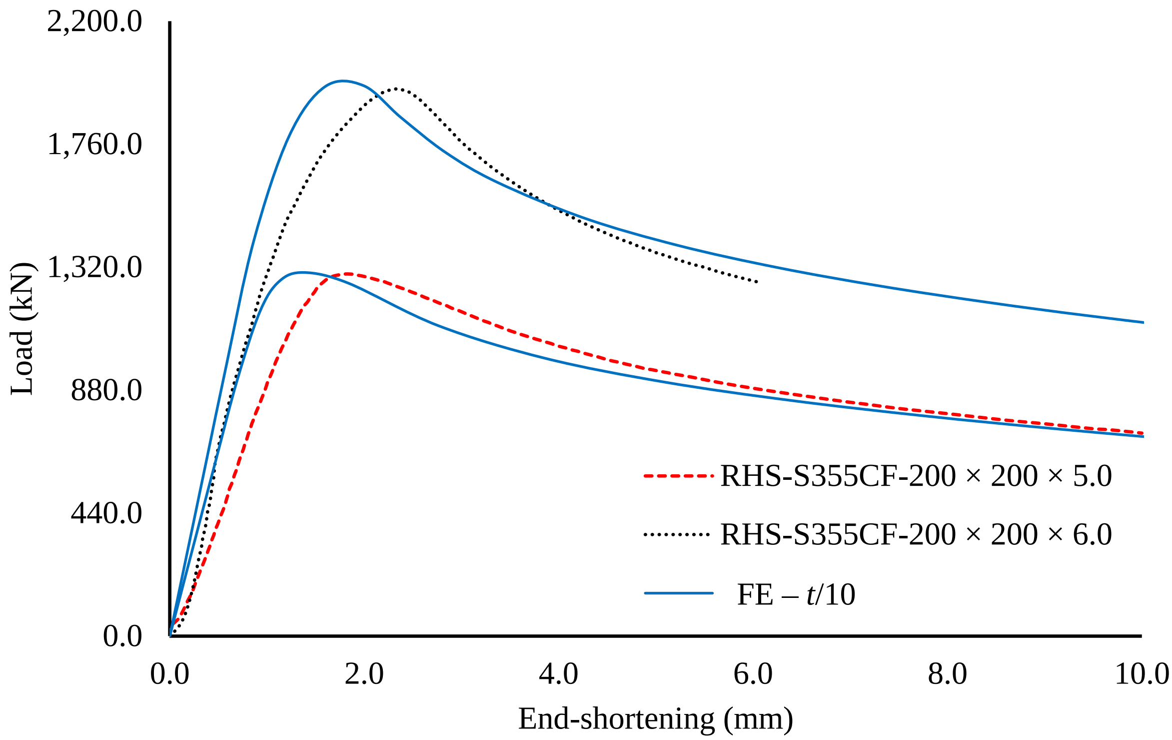

Fig. 10. Comparison of test (reported by Nseir [37]) and FE load-end shortening curves for cold-formed steel stub columns.

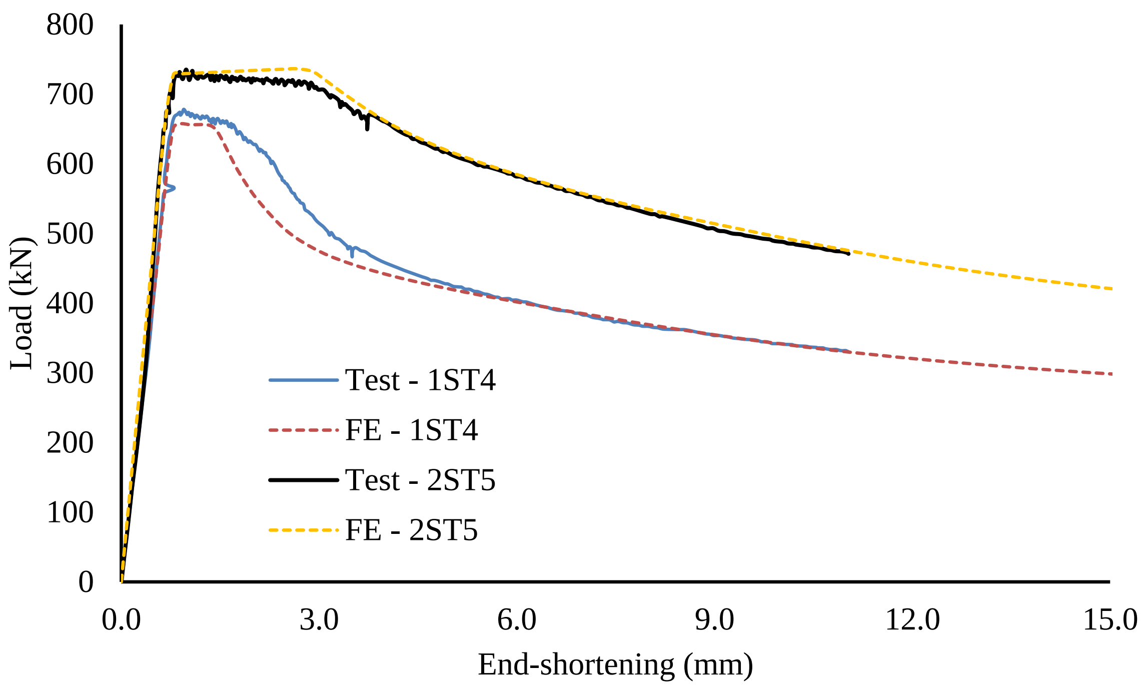

Fig. 11. Comparison of test (reported by Liew [38]) and FE load-end shortening curves for hot-rolled steel stub columns.

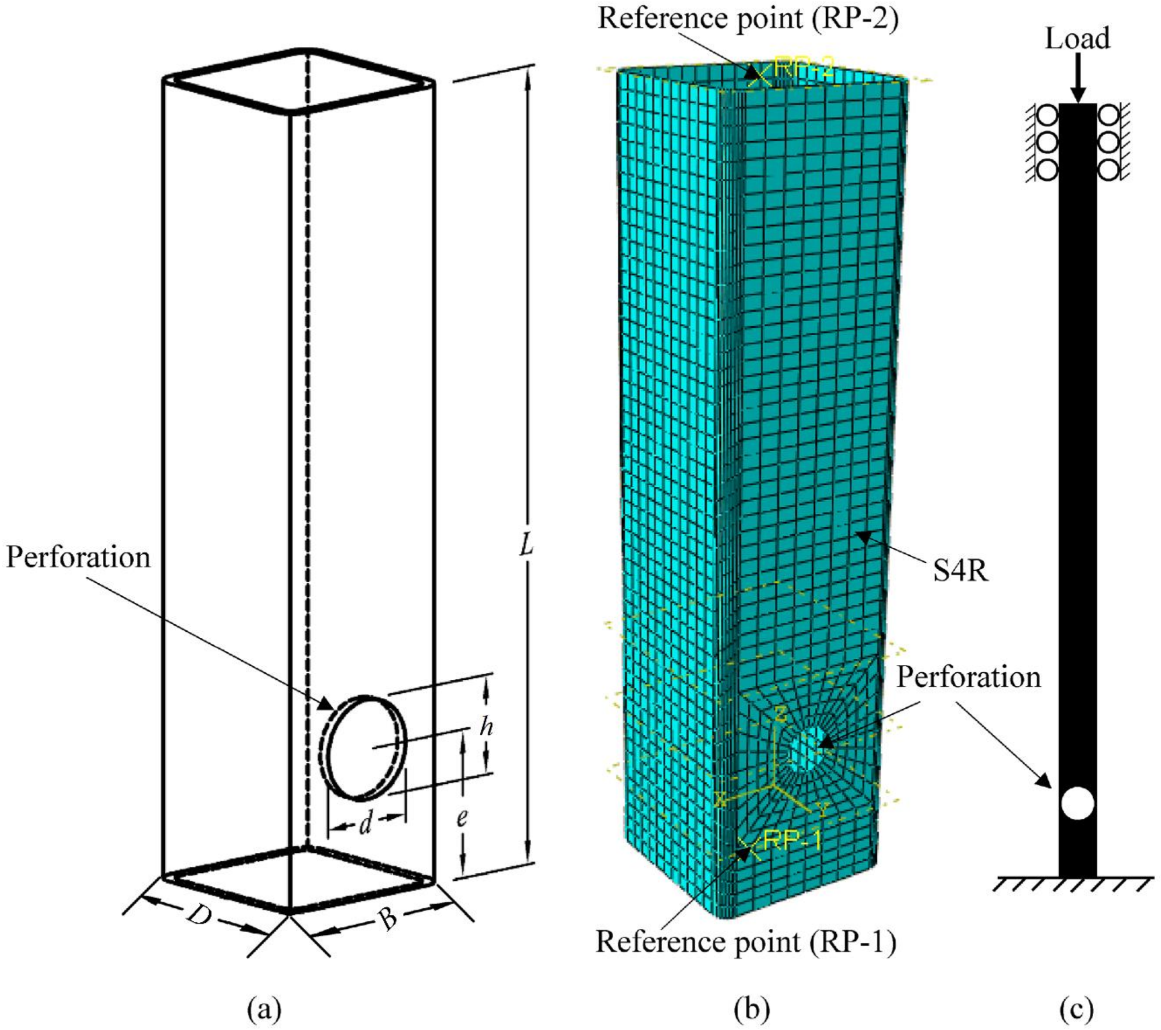

Fig. 12. Typical (a) geometry (b) FE Model and (c) boundary and loading conditions of a single side perforated stub column.

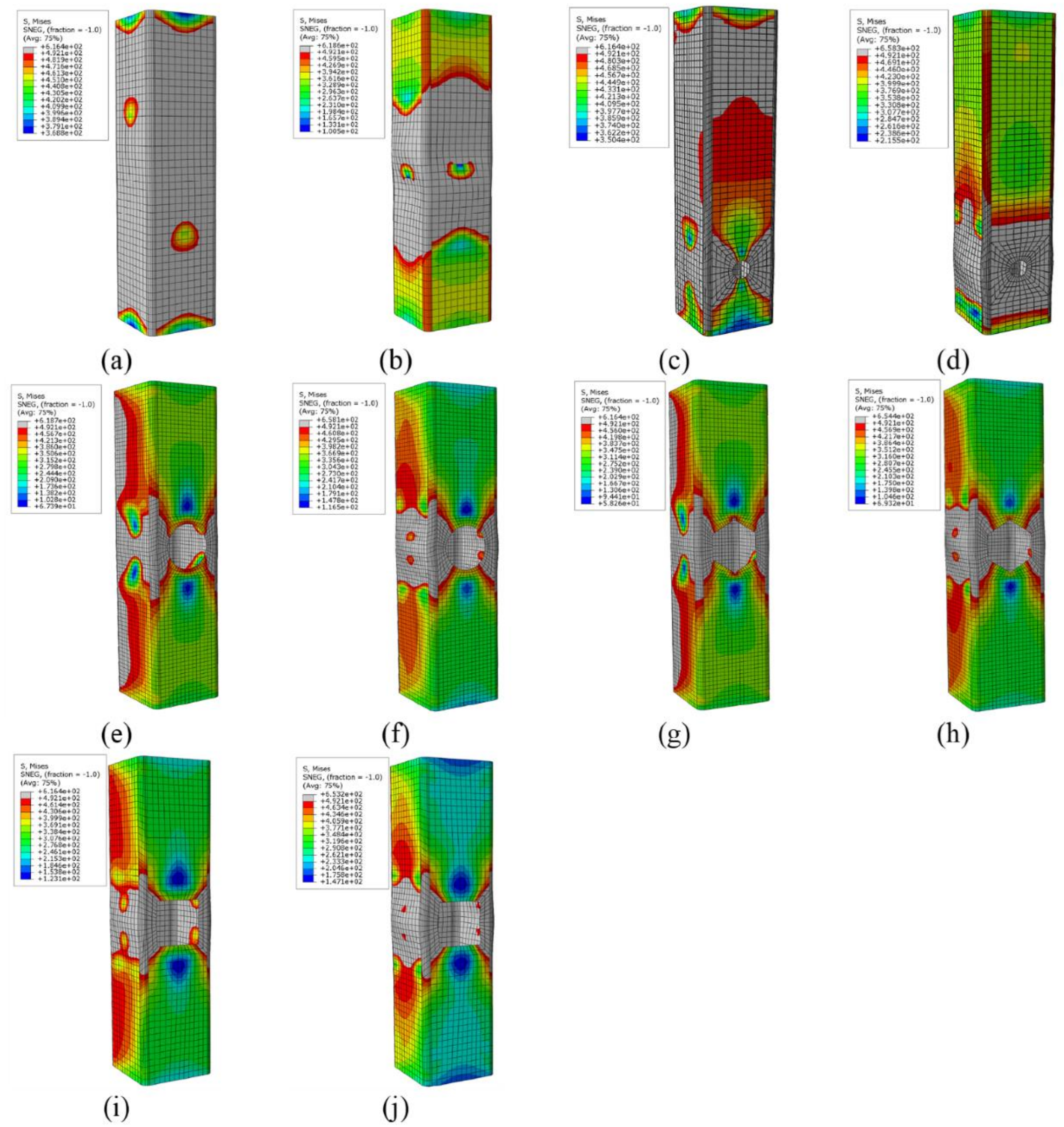

Fig. 13. Typical deformed shapes (superimposed with Von-Mises stress contour) for cold-formed steel, with t = 8.5 mm (Class 1–3), (a) unperforated stub column at $\delta = \delta_u$ (ultimate load), (b) unperforated stub column at $\delta = 1.5\delta_u$, (c) stub column with circular perforation (with d/w = 0.3 and e/L = 0.2) at $\delta = \delta_u$, (d) stub column with circular perforation (with d/w = 0.3 and e/L = 0.2) at $\delta = 1.5\delta_u$, (e) stub column with circular perforation (with d/w = 0.7 and e/L = 0.5) at $\delta = \delta_u$, (f) stub column with circular perforation (with d/w = 0.7 and e/L = 0.5) at $\delta = 1.5\delta_u$, (g) stub column with hexagonal perforation (with d/w = 0.7 and e/L = 0.5) at $\delta = \delta_u$, (h) stub column with hexagonal perforation (with d/w = 0.7 and e/L = 0.5) at $\delta = 1.5\delta_u$, (i) stub column with square perforation (with d/w = 0.7 and e/L = 0.5) at $\delta = \delta_u$, (j) stub column with square perforation (with d/w = 0.7 and e/L = 0.5) at $\delta = 1.5\delta_u$.

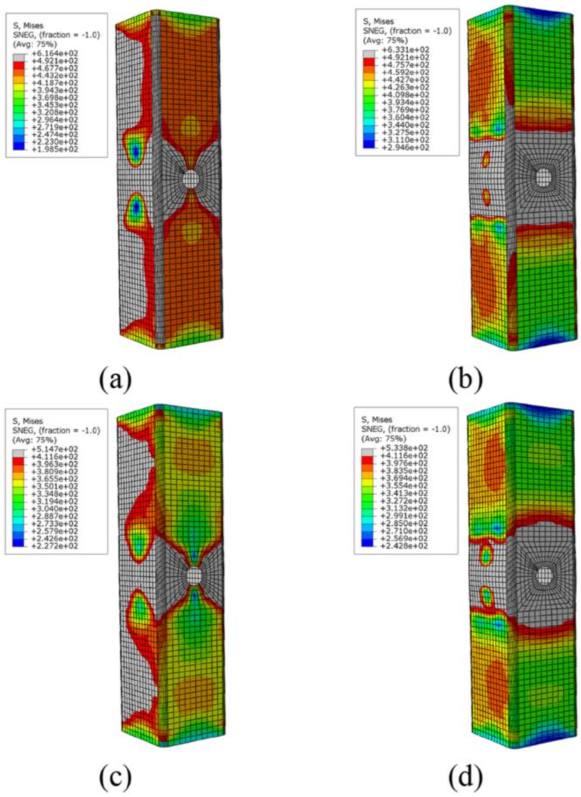

Fig. 14. Typical deformed shapes along with Von-Mises stress contour, considering circular perforation with *d*/*w* = 0.3 located *e*/*L* = 0.5, having cross-section thickness of 8.5 mm (Class 1–3) for: (a) cold-formed steel stub column at $\delta = \delta_u$, (b) cold-formed steel stub column at $\delta = 1.5\delta_u$, (c) hot-rolled steel stub column at $\delta = \delta_u$, (d) hot-rolled steel stub column at $\delta = 1.5\delta_u$.

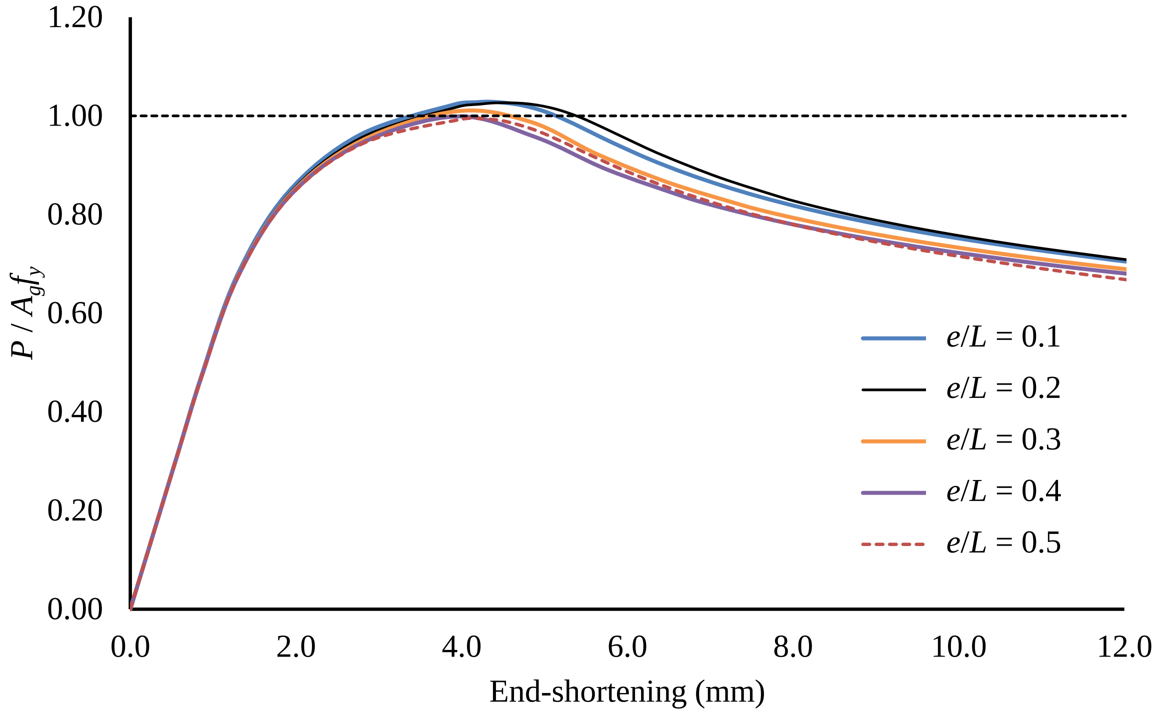

Fig. 15. Load versus end-shortening curves for different values of eccentricity considering circular perforation of d/w = 0.5 and t = 8.5 (Class 1–3), for cold-formed steel column.

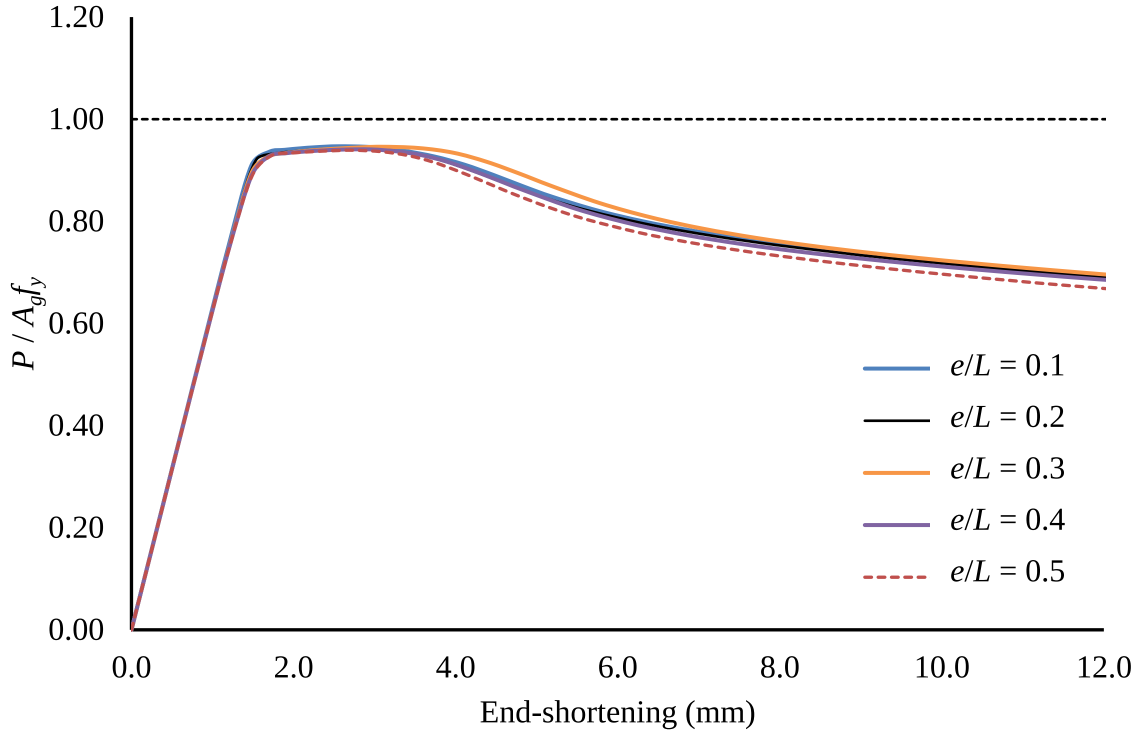

Fig. 16. Load with end-shortening curves for different values of eccentricity considering circular perforation of d/w = 0.5 and t = 8.5 (Class 1–3), for hot-rolled steel column.

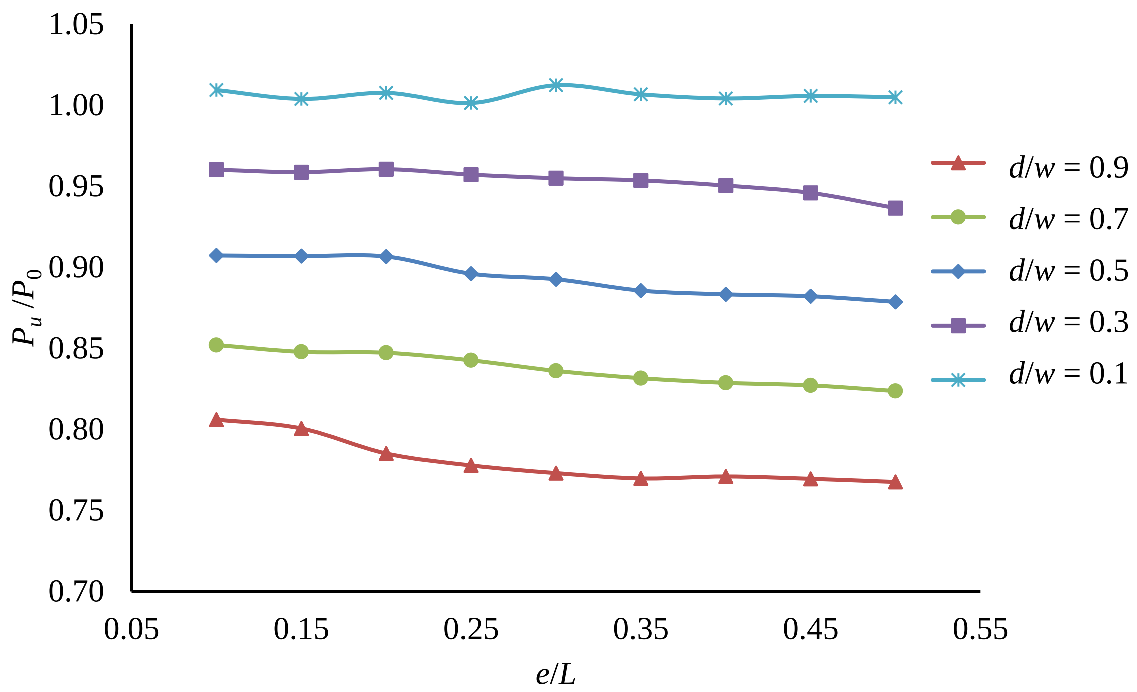

Fig. 17. Variation of P_u /P_0 over e/L for Class 1–3 perforated cold-formed steel module column having circular shape perforation of various d/w.

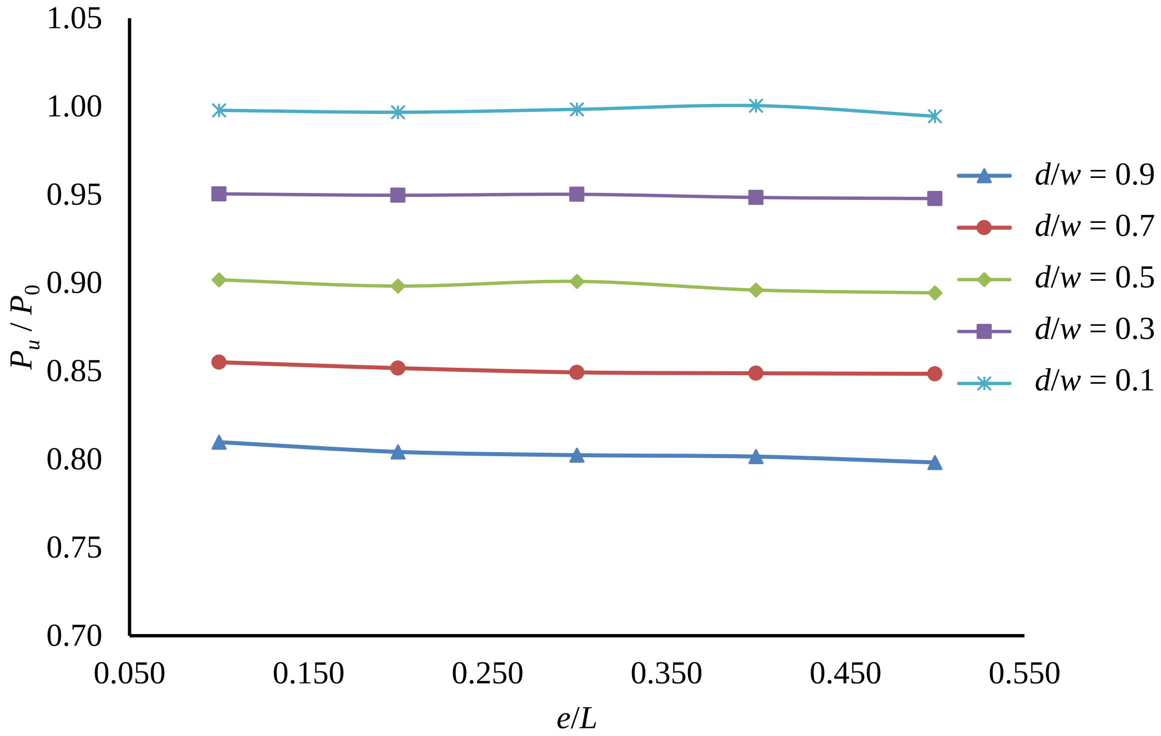

Fig. 18. Variation of P_u / P_0 over e/L for Class 1–3 perforated hot-rolled steel module column having circular shape perforation of various d/w.

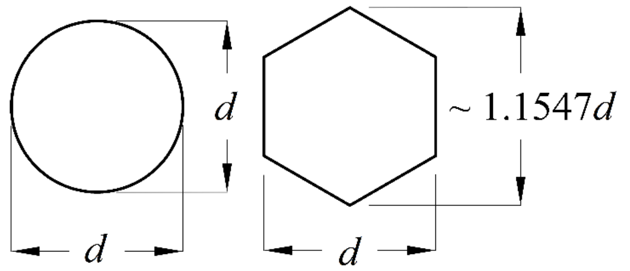

Fig. 19. Perforation shapes considered in the present study.

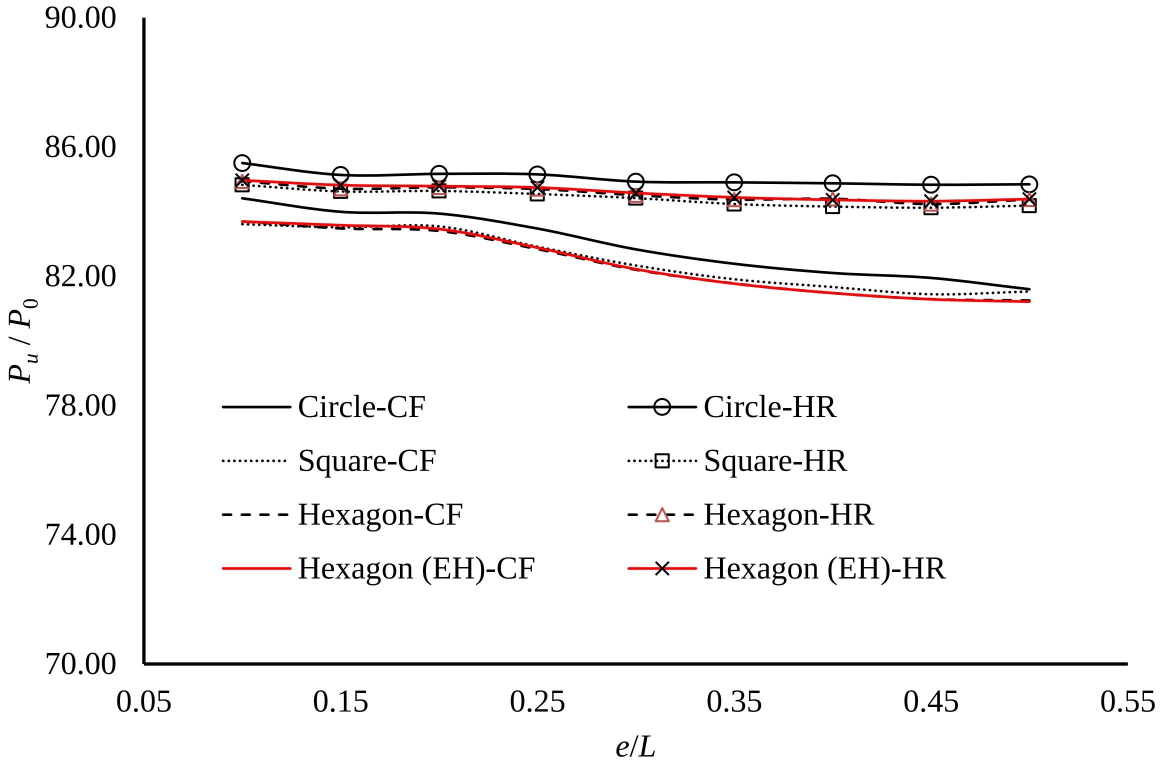

Fig. 20. Variation of P_u / P_0 versus e/L for different perforation shapes, *viz*, Circular, Square and hexagonal shapes, considering Class 1–3 cross-section and d/w = 0.7.

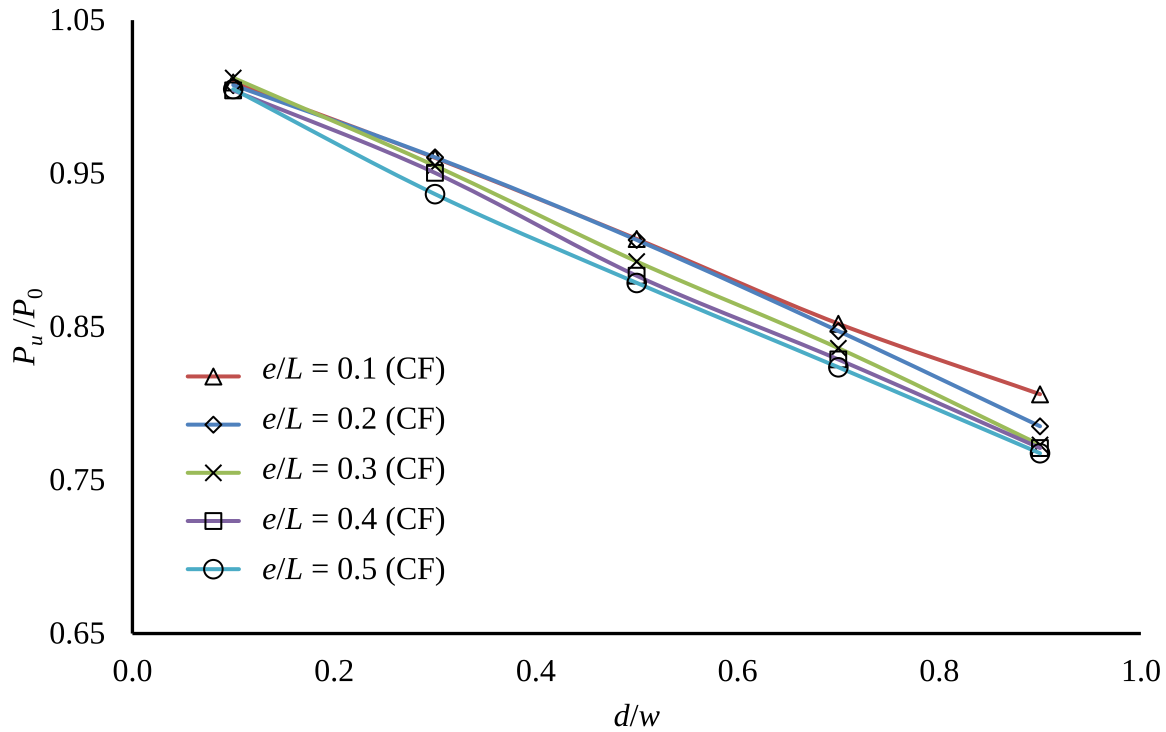

Fig. 21. Variation P_u/P_0 with d/w considering cold-formed steel cross-section of t = 8.5 mm (Class 1–3) having circular perforation for different eccentricities ($0.1 \leq e/L \leq 0.5$).

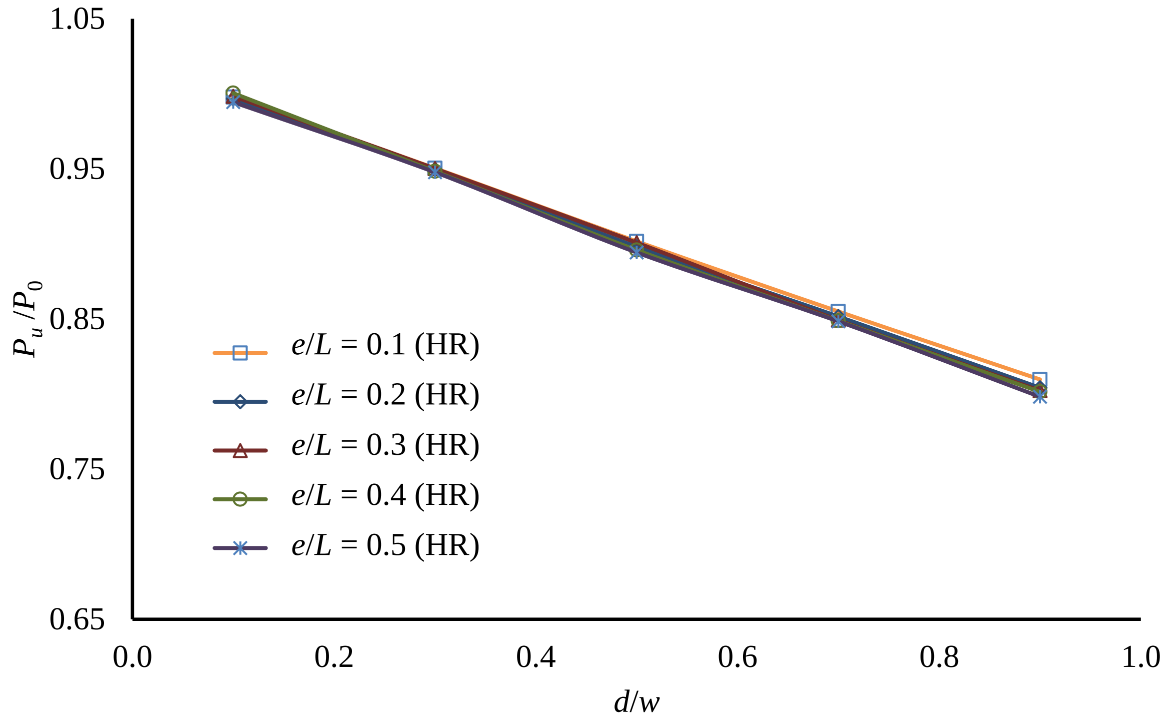

Fig. 22. Variation P_u/P_0 with d/w considering hot-rolled steel cross-section of t = 8.5 mm (Class 1–3) having circular perforation for different eccentricities ($0.1 \leq e/L \leq 0.5$).

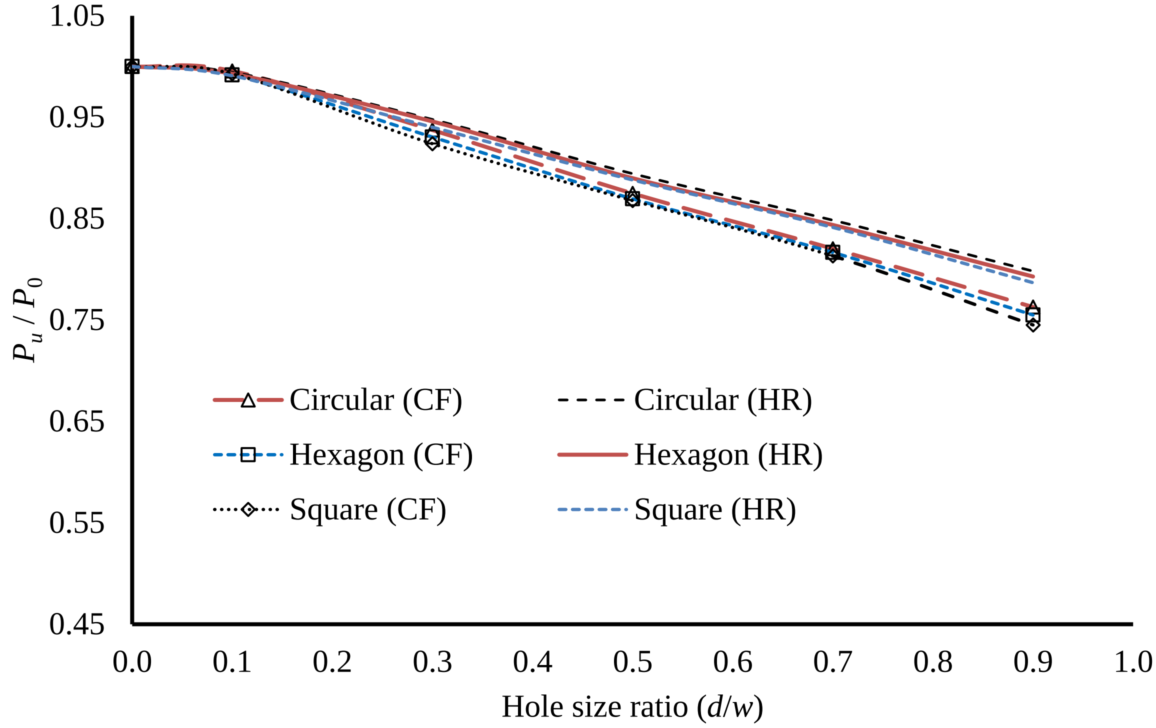

Fig. 23. Effect of *d*/*w* for Class 1–3 cross-sections.

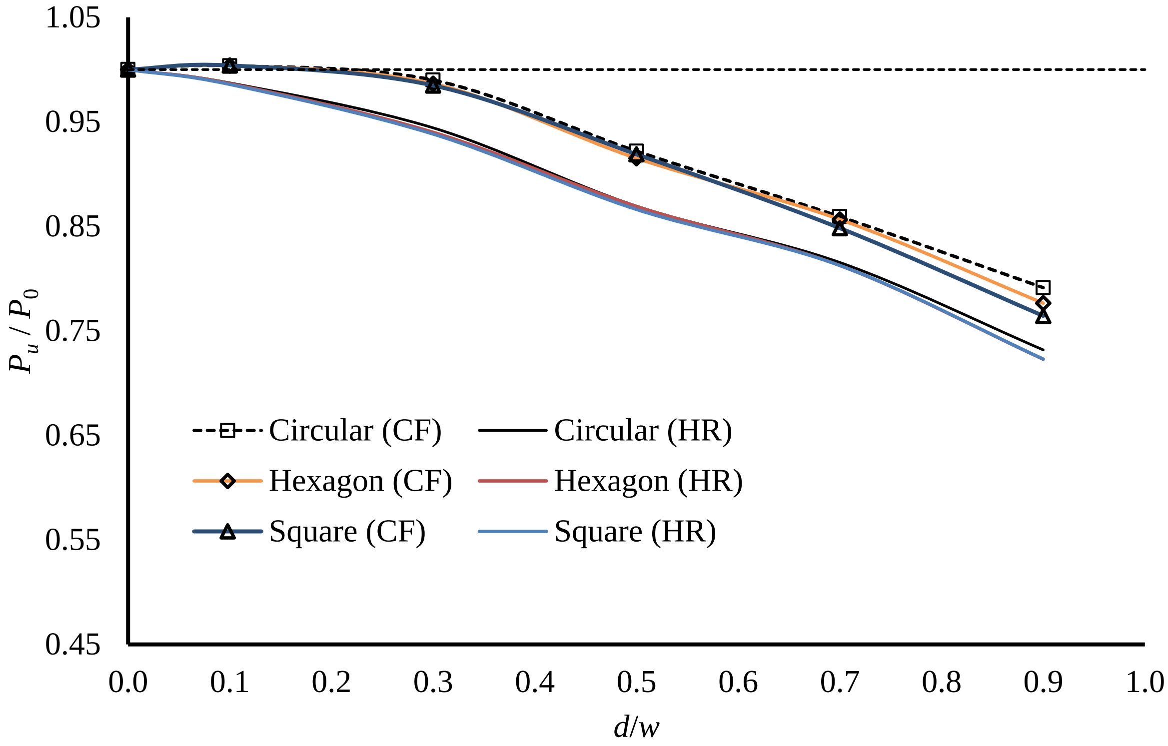

Fig. 24. Effect of *d*/*w* for Class 4 cross-sections.

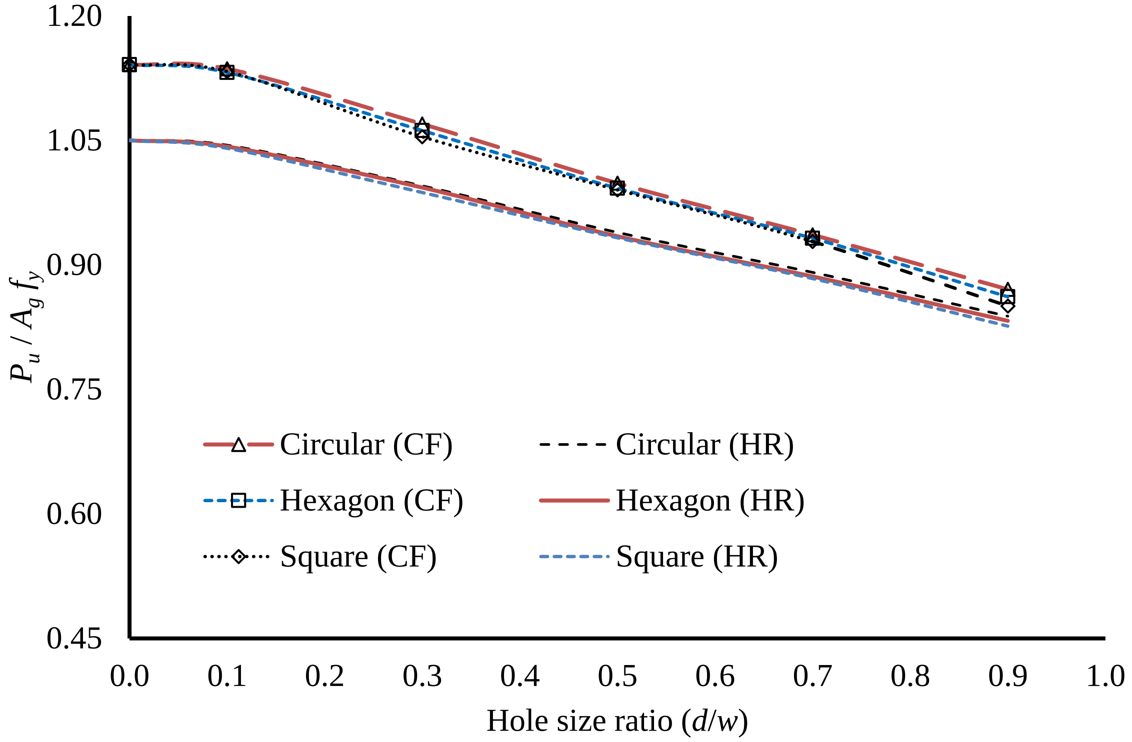

Fig. 25. Comparison of the performance of cold-formed and hot-rolled steel module stub columns for Class 1–3 cross-sections.

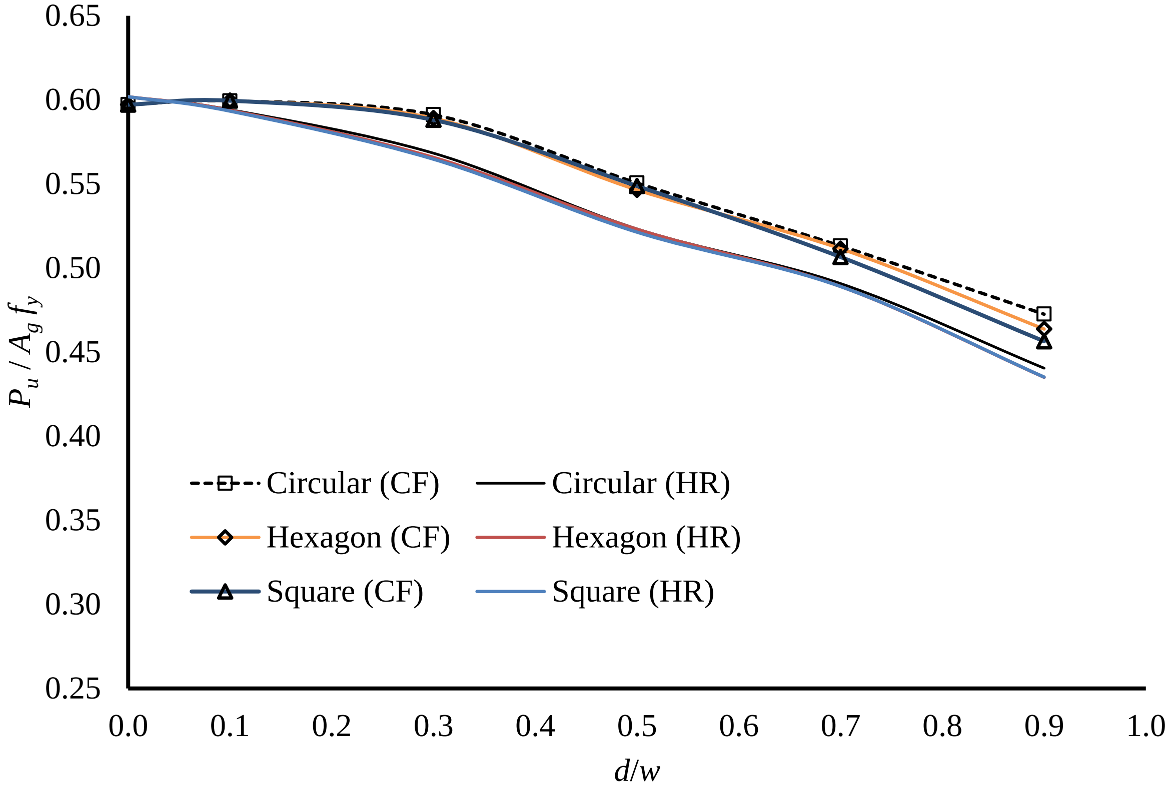

Fig. 26. Comparison of the performance of cold-formed and hot-rolled steel module stub columns for Class 4 cross-sections.

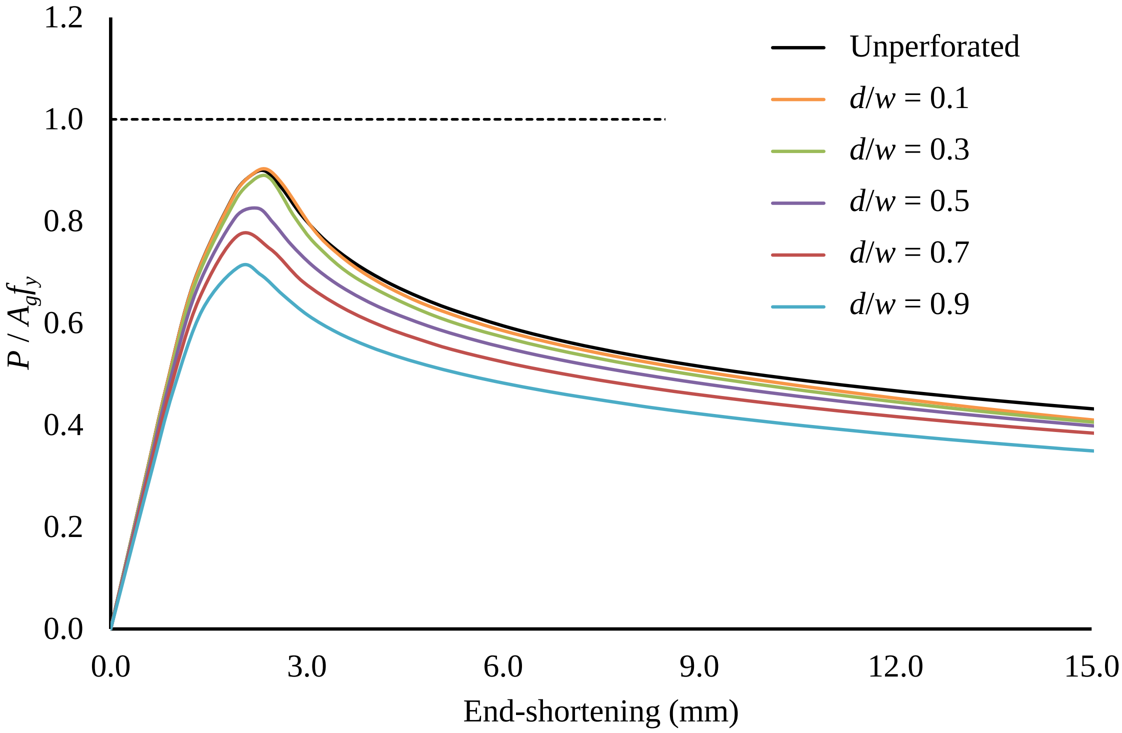

Fig. 27. Load versus end-shortening curves of perforated cold-formed steel columns having circular cut-outs of various d/w, located at e/L = 0.5 and t = 5.5 (Class 4).

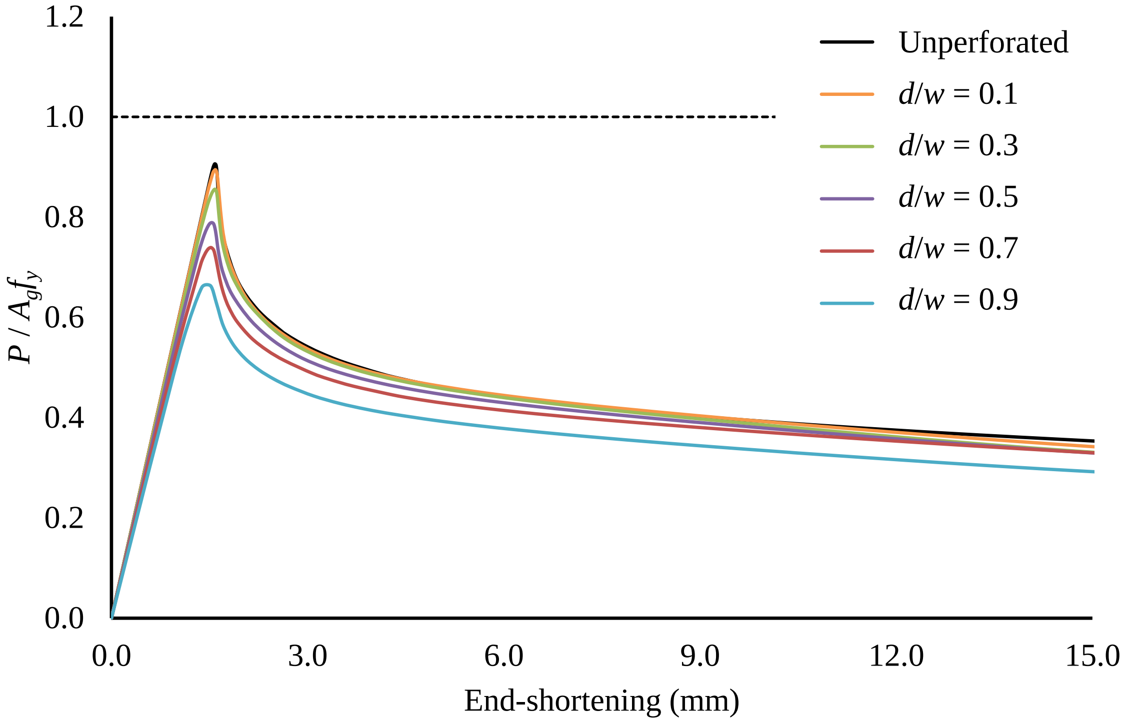

Fig. 28. Load versus end-shortening curves of perforated hot-rolled steel module columns having circular cut-outs of various d/w, located at e/L = 0.5 and t = 5.0 (Class 4).

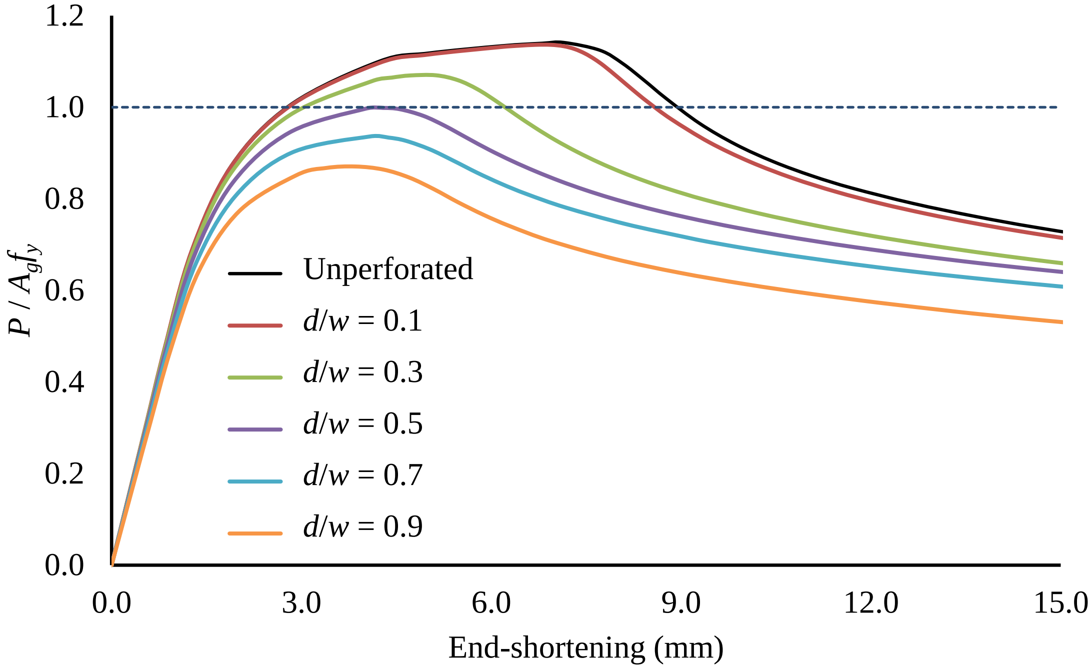

Fig. 29. Load with end-shortening curves of perforated cold-formed steel module columns having circular cut-outs of various *d*/*w*, located at *e*/*L* = 0.5 and *t* = 8.5 (Class 1–3).

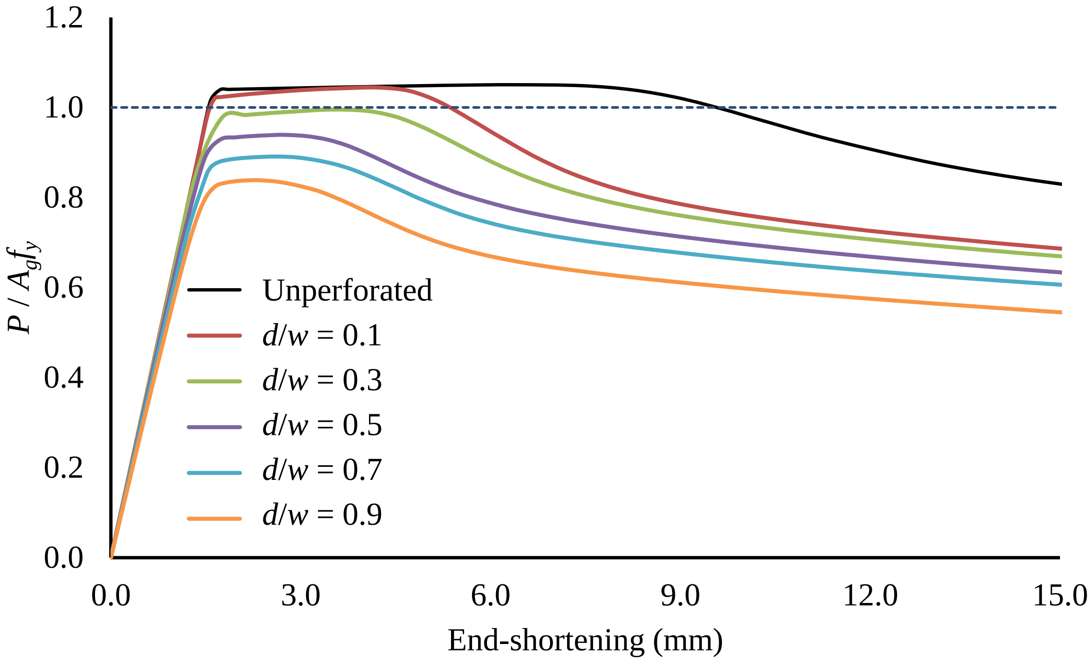

Fig. 30. Load with end-shortening curves of perforated hot-rolled steel module columns having circular cut-outs of various *d*/*w*, located at *e*/*L* = 0.5 and *t* = 8.5 (Class 1–3).

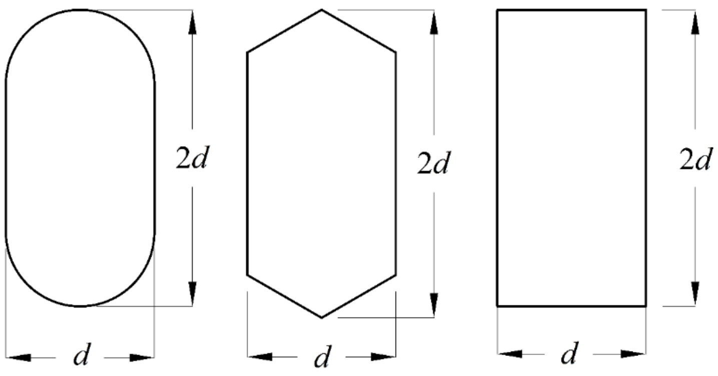

Fig. 31. Typical elongated perforation shapes when the aspect ratio is 2.0 (i.e. *h*/*d* = 2.0).

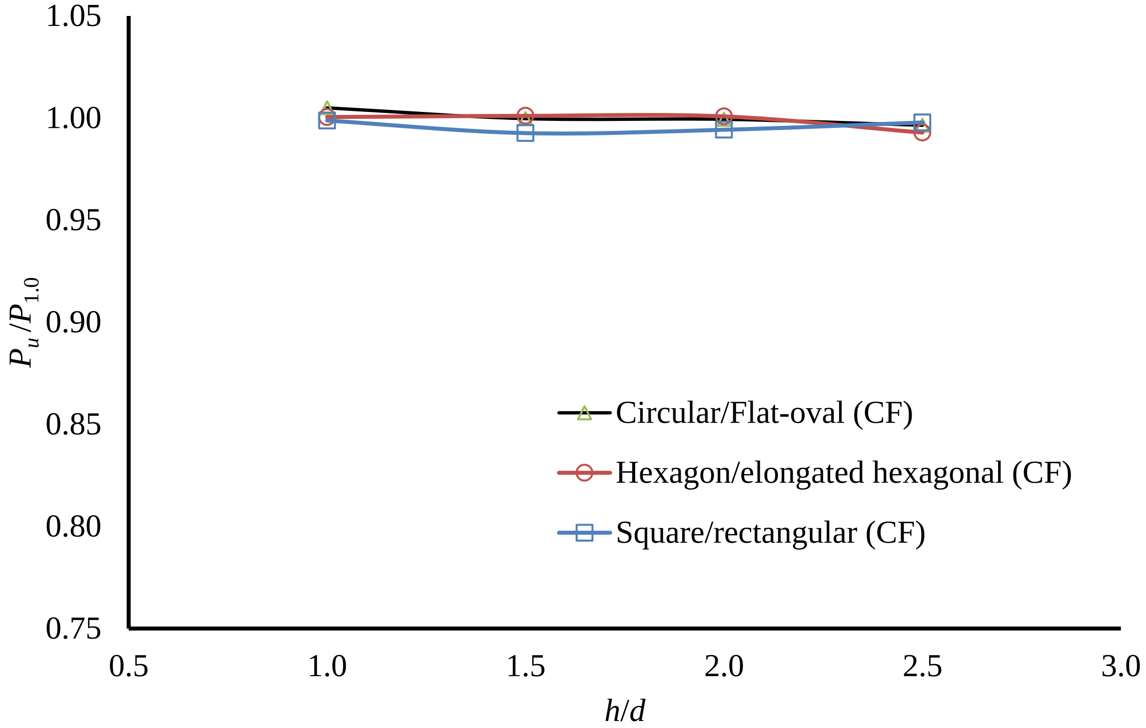

Fig. 32. Effect of perforation height for various aspect ratio (i.e. *h*/*d* = 1.0–2.5) on perforated cold-formed steel module columns.

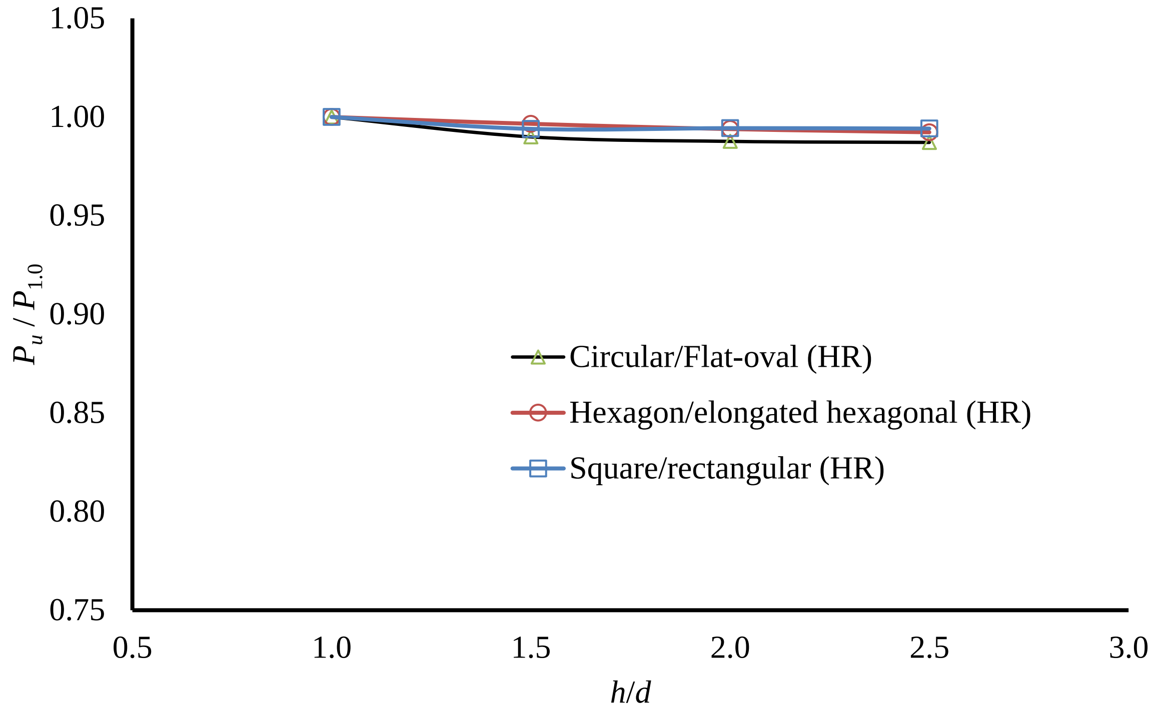

Fig. 33. Effect of perforation height for various aspect ratio (i.e. *h*/*d* = 1.0–2.5) on perforated hot-rolled steel module columns.

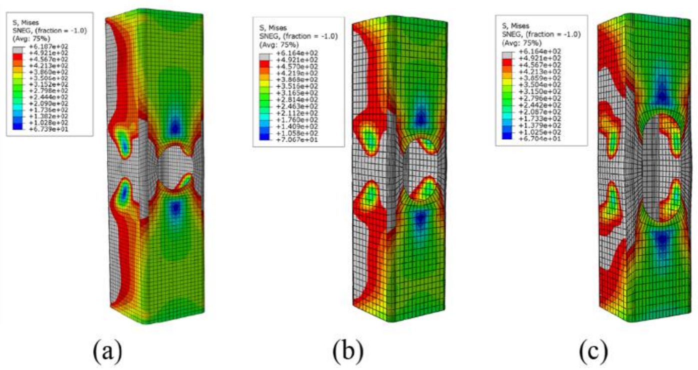

Fig. 34. Von Mises stress contour (superimposed with deformed shapes) for perforated stub column with d/w =0.7 and t = 8.5 mm (Class 1–3) having: (a) circular perforation of h/d =1.0 and deformation, $\delta = \delta_u$, (b) circular (flat-oval) perforation of h/d =1.5 and deformation, $\delta = \delta_u$ and (c) circular (flat-oval) perforation of h/d =2.5 and deformation, $\delta = \delta_u$.

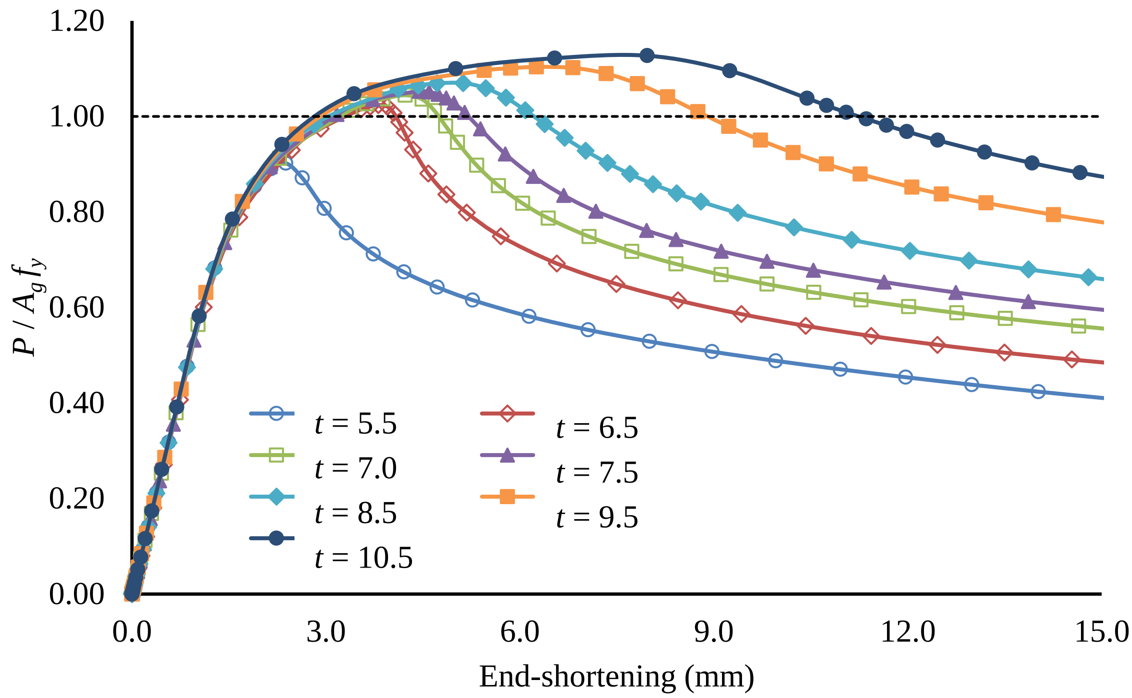

Fig. 35. Variation of normalised load versus end-shortening curves for cold-formed steels for different values of thickness and d/w = 0.3.

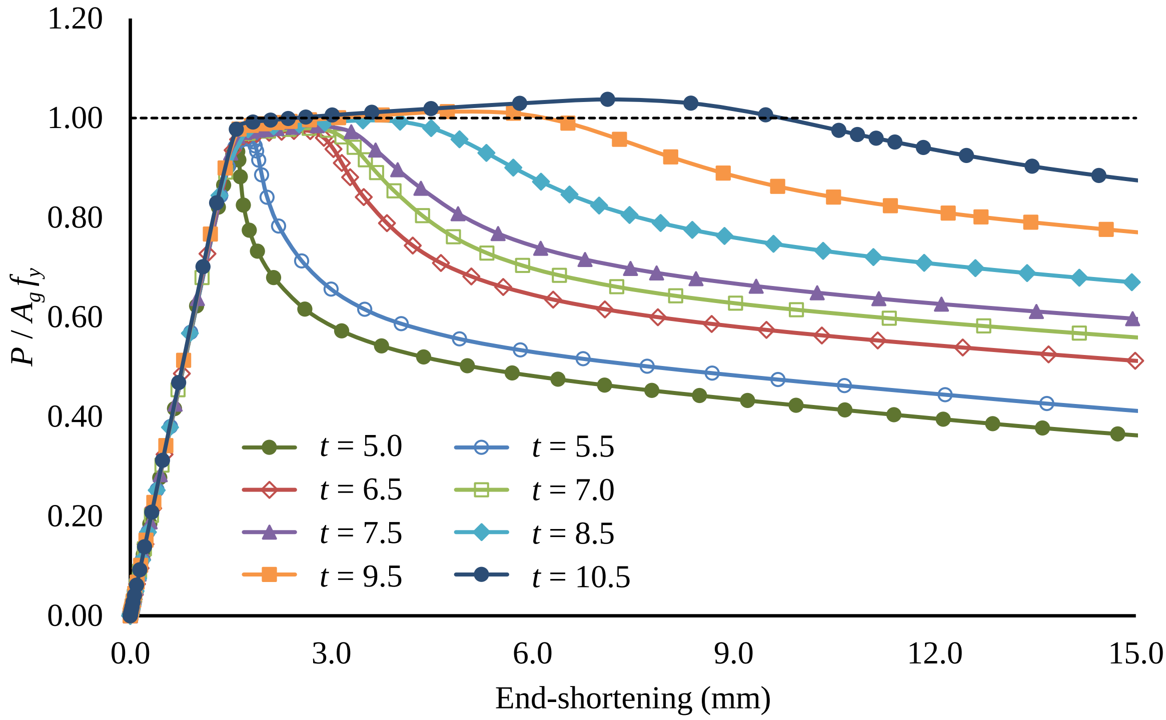

Fig. 36. Variation of normalised load versus end-shortening curves for hot-rolled steels for different values of thickness and d/w = 0.3.

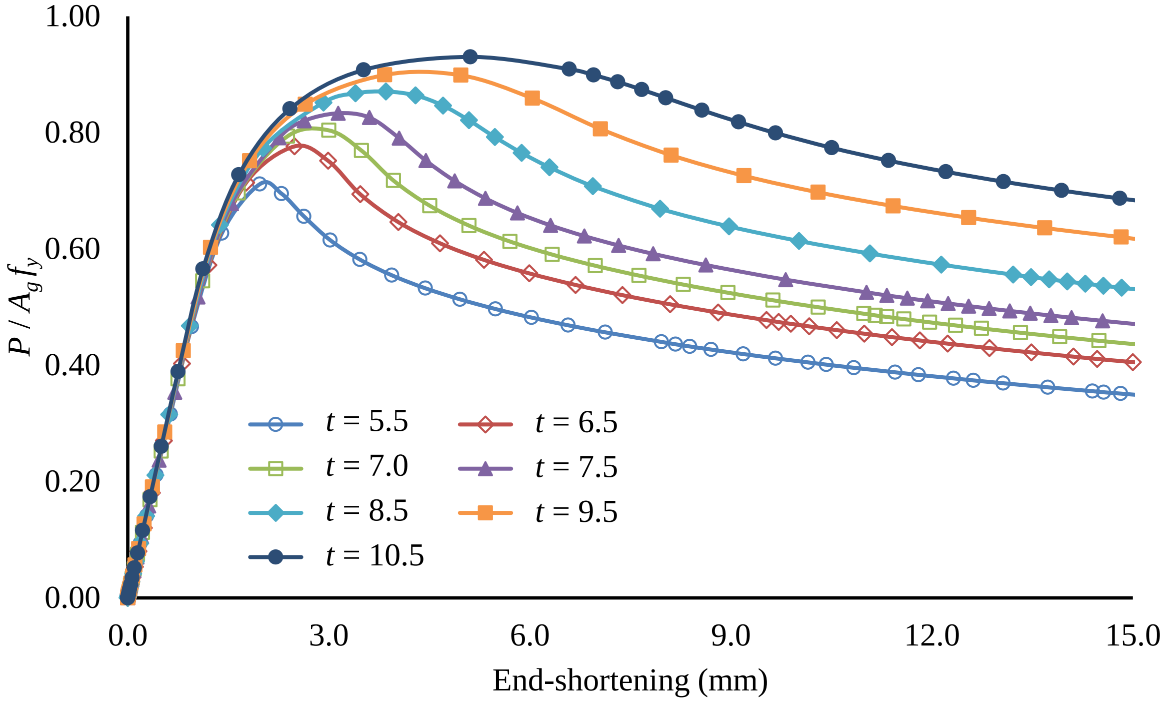

Fig. 37. Variation of normalised load versus end-shortening curves for cold-formed steels for different values of thickness and d/w = 0.9.

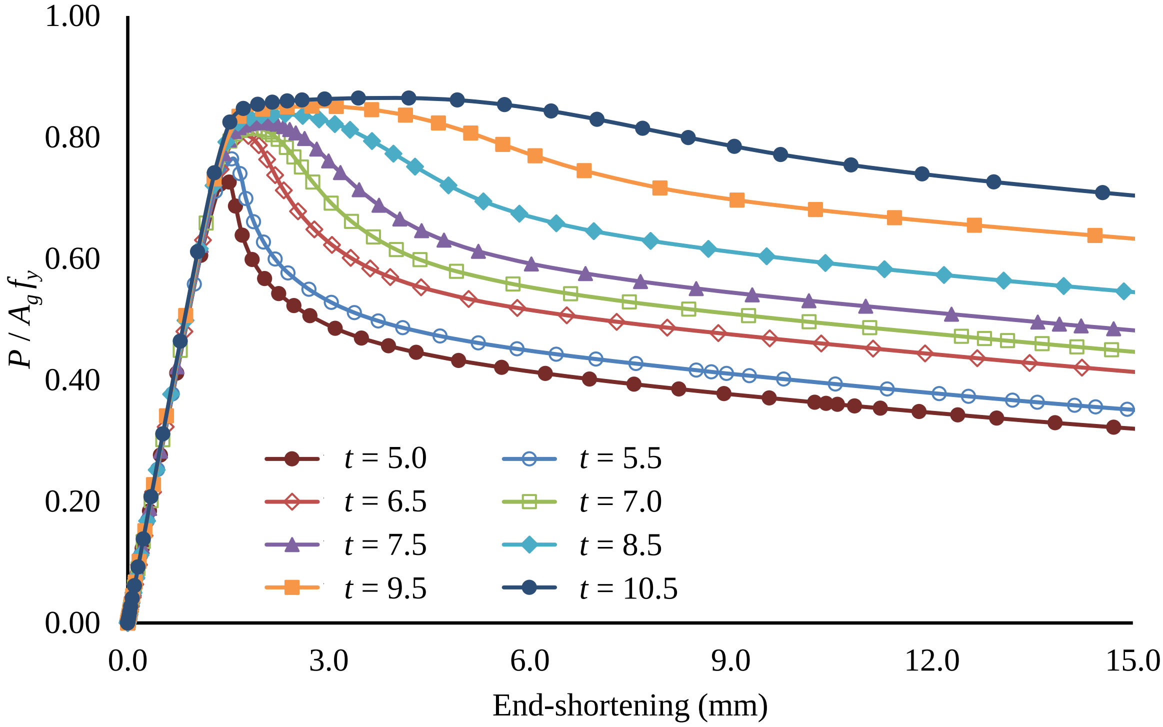

Fig. 38. Variation of normalised load versus end-shortening curves for hot-rolled steels for different values of thickness and d/w = 0.9.

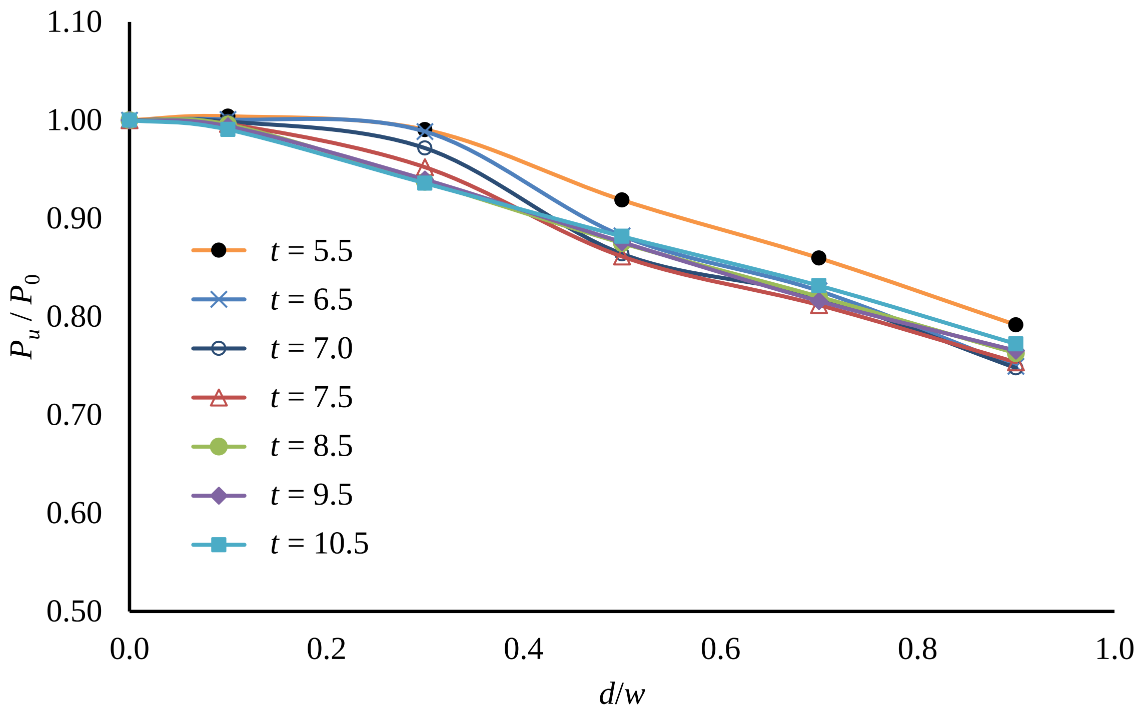

Fig. 39. Effect of section thickness covering Class 1–4 cross-sections for cold-formed steel module columns.

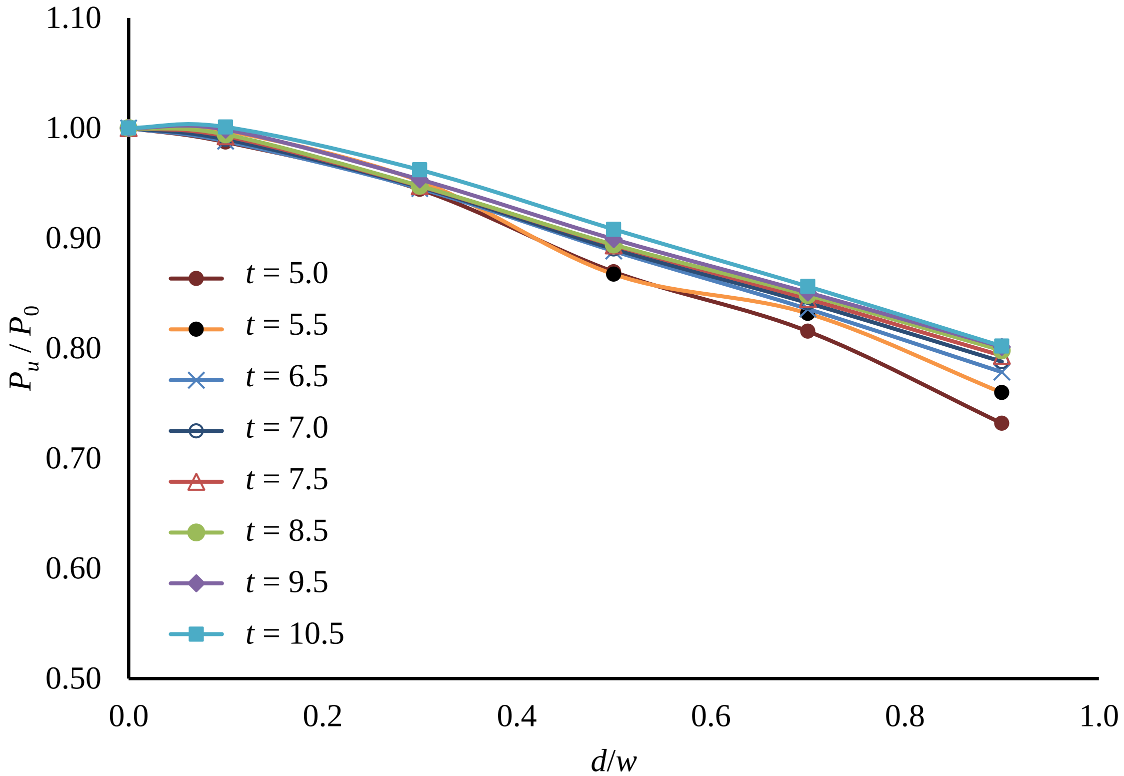

Fig. 40. Effect of section thickness covering Class 1–4 cross-sections for hot-rolled steel module columns.